RBPMS2 is a conserved regulator of alternative splicing that promotes myofibrillar organization and optimal calcium handling in cardiomyocytes

Alexander A. Akerberg (PhD)[1,2,3], Michael Trembley (PhD)[1,3], Vincent Butty (MD, PhD)[4], Asya Schwertner (PhD)[2,3], Long Zhao (PhD)[2,3], Manu Beerens (PhD)[2,3,5], Xujie Liu (PhD)[1,3], Mohammed Mahamdeh (PhD)[2,3], Shiaulou Yuan (PhD)[2,3], Laurie Boyer (PhD)[4,6], Calum MacRae (MD, PhD)[3,5], Christopher Nguyen (PhD)[2,3], William T. Pu (MD)[1,3,7], Caroline E. Burns (PhD)[1,2,3,7*], C. Geoffrey Burns (PhD)[1,2,3*]

[1] Division of Basic and Translational Cardiovascular Research, Department of Cardiology, Boston Children's Hospital, Boston, MA, USA
[2] Cardiovascular Research Center, Massachusetts General Hospital, Charlestown, MA, USA
[3] Harvard Medical School, Boston, MA, USA
[4] Department of Biology, Massachusetts Institute of Technology, Cambridge, MA, USA
[5] Division of Cardiovascular Medicine, Brigham and Women's Hospital, Boston, MA, USA
[6] Department of Biological Engineering, Massachusetts Institute of Technology, Cambridge, MA, USA
[7] Harvard Stem Cell Institute, Cambridge, MA, USA

* Correspondence: Caroline and C. Geoffrey Burns: caroline.burns@childrens.harvard.edu, geoff.burns@childrens.harvard.edu. 300 Longwood Ave., Boston MA 02115

Current Word Count: 10,455
AHA Subject Terms: Contractile function, myocardial biology, Genetics, Gene expression and regulation, Heart failure

ABSTRACT

Rationale: The identification of novel cardiomyocyte-intrinsic factors that support heart function will expand the number of candidate genes and therapeutic options for heart failure, a leading cause of death worldwide.

Objective: To identify and characterize conserved regulators of cardiomyocyte function.

Methods and Results: We report that the RNA-binding protein RBPMS2 is required for myofibril organization and the regulation of intracellular calcium dynamics in both zebrafish embryos and human induced pluripotent stem cell-derived cardiomyocytes (hiPSC-CMs). A differential expression screen in zebrafish uncovered enrichment of *rbpms2* paralogs, *rbpms2a* and *rbpms2b,* in the myocardium. Double knock-out (*rbpms2*-null) embryos suffer from compromised ventricular filling during the relaxation phase of the cardiac cycle, which significantly reduces cardiac output. Whole transcriptome sequencing and validation studies revealed differential alternative splicing of several genes linked to cardiomyopathies in humans, including *myosin binding protein C3* (*mybpc3*) and *phospholamban* (*pln*), consistent with a role in causing the observed ventricular deficiencies. Further, *RBPMS*2-null hiPSC-CMs exhibit myofibril and calcium handling defects that are highly analogous to those observed in the *rbpms2*-null zebrafish ventricle.

Conclusions: Taken together, our data identify *RBPMS2* as a conserved and essential regulator of alternative splicing that is required for myofibrillar organization and optimal calcium handling from zebrafish to humans.

INTRODUCTION

Heart failure remains a common, costly, and growing public health burden [1]. While lifestyle choices that cause hypertension and myocardial infarction are substantial contributors to heart failure, inherited and *de novo* genetic mutations that cause primary diseases of the heart muscle, including hypertrophic cardiomyopathy (HCM) and dilated cardiomyopathy (DCM) are also important instigators of disease [2,3]. Causal mutations for HCM and DCM commonly reside within two classes of genes, those encoding components of the sarcomere, the basic contractile unit of cardiac muscle, and those encoding factors that regulate calcium handling, another critical determinant of cardiac contractility [2,4–6]. While the pathogenesis of mutations affecting sarcomeres and calcium handling is well-established in HCM and DCM, a significant percentage of cases remain idiopathic, because clinically recognized cardiomyopathy susceptibility genes remain mutation free in targeted sequencing panels. Therefore, ongoing efforts to identify novel molecular activities required for optimal myocardial contractility will highlight novel candidate genes for primary cardiomyopathies.

Alternative mRNA splicing has emerged in recent years as an important regulator of myocardial contractility in humans. Disruptions in the RNA-recognition motif (RRM)-containing protein RBM20 were recently discovered to cause dilated cardiomyopathy (DCM) by regulating alternative splicing of TITIN (TTN), the largest protein component of the sarcomere [7–9]. TTN transcripts within the heart can be separated into three distinct classes, each of which codes for a unique combination of functional domains [10]. Loss of Rbm20 in animal models results in aberrant splicing of TTN, leading to changes in ventricular morphology and diminished contractility in a manner consistent with observations in DCM patients. Clinical studies have further confirmed that genetic variation in the Rbm20 locus is associated with a higher risk of cardiomyopathy [11,12]. Alternatively, spliced transcripts of calcium/calmodulin-dependent kinase II delta (CAMK2D) were also shown to contribute to increased risk of arrhythmogenic cardiomyopathy in the absence of Rbm20 [7], demonstrating roles for Rbm20 in the regulation of

82 myocardial calcium handling and action potential propagation. Similar to Rbm20, another RRM-
83 containing protein, termed Rbm24, was shown to regulate the splicing of a subset of genes
84 encoding components of the sarcomere, including TTN, within postnatal mice[13]. Initial screens
85 for Rbm24 mutations in human cardiomyopathy patients suggest a potential link to disease,
86 however, these mutations were found to be relatively rare in the disease population [14]. Together
87 these data represent the first etiological links between splicing factors and cardiomyopathy,
88 thereby underscoring the importance for further research to identify the full array of splicing
89 factors that regulate cardiac form and function.

90 The importance of alternative splicing in the heart is further evidenced by the abundance
91 of isoform variation within cardiac-specific transcripts. Furthermore, many genes with
92 established roles in cardiomyopathy are known to produce multiple distinct isoforms within the
93 heart. For example, the cardiac troponin t (*TNNT2*) gene is alternatively spliced in a regulated
94 pattern during cardiac development and aberrant splicing can lead to cardiomyopathy in animal
95 models [15–17]. Other cardiomyopathy genes such as tropomyosin (*TPM1*) and myosin binding
96 protein C3 (*MYBPC3*) are predicted to be alternatively spliced in a similar fashion, however the
97 importance of these splicing events and the identity of the factors that govern them remain
98 unknown.

99 Here, we identify the RRM-containing protein Rbpms2 (RNA binding protein with multiple
100 splicing 2) as a crucial regulator of alternative splicing within the developing myocardium. We
101 show that Rbpms2a and Rbpms2b redundantly promote ventricular contractility within the
102 developing zebrafish heart. Further, we show that these Rbpms2 proteins regulate the splicing
103 of numerous genes that are associated with cardiac sarcomere assembly and ion transport,
104 including transcripts for known disease genes *mybpc3* and *phospholamban* (*pln)* [18,19]. We then
105 demonstrate that *rbpms2*-null animals exhibit sarcomere disorganization and calcium handling
106 deficits that are consistent with the misregulation of Rbpms2 targets.
107

METHODS

Data availability

All data and materials will be made publicly available upon publishing. RNA-sequencing datasets summarized in Tables S1-5 were deposited into the NCBI GEO repository under accession numbers GSE167416 and GSE167414.

Zebrafish husbandry and strains

Zebrafish were bred and maintained following animal protocols approved by the Institutional Animal Care and Use Committees at Massachusetts General Hospital and Boston Children's Hospital. All protocols and procedures followed the guidelines and recommendations outlined by the Guide for the Care and Use of Laboratory Animals. The following zebrafish strains were used in this study: *TgBAC(-36nkx2.5:ZsYellow)*^{fb7} [20], *Tg(myl7:GFP)*^{fb1} [formerly *Tg(cmlc2:GFP)*^{fb1}*]* [21], *Tg(myl7:NLS-eGFP)*^{fb18} [formerly *Tg(cmlc2:nucGFP)*^{fb18}*]* [22], *Tg(myl7:actn3b-EGFP)*^{sd10} [formerly *Tg(cmlc2:actinin3-EGFP)]* [23], *rbpms2a*^{chb3} (this study), and *rbpms2b*^{chb4} (this study).

Generation and genotyping of *rbpms2a*^{ch3} and rbpms2*b*^{ch4} mutant alleles

Customized transcription activator-like effector nucleases (TALENs) [24–26] were used to induce double-stranded breaks in regions of the *rbpms2a* and *rbpms2b* loci that encode the RNA-recognition motifs. TALENs were designed to bind the sequences 5'-TGCCTGTTGACATCAAGC-3' (+) and 5'-TTGAAGGGTCTGAACAGC-3' (-) in exon 2 of *rbpms2a* and 5'- TGCCAACAGATATCAAAC-3' (+) and 5'-TTAAATGGTCGAAATAGC-3' (-) in exon 2 of *rbpms2b*. TALEN constructs were constructed as described [26]. Messenger RNAs encoding each TALEN pair were produced in vitro and co-injected into one-cell stage zebrafish embryos as described [25] Germline transmission of TALEN-induced mutations was detected using fluorescent PCR and DNA-fragment analysis as described [27]. The nucleotides deleted in

134 the mutant alleles *rbpms2a*^{chb3} and *rbpms2b*^{chb4} are shown (Fig. S4A,B). The primers utilized to
135 distinguish wild-type *rbpms2a* and *rbpms2b* from the mutant alleles *rbpms2a*^{chb3} and
136 *rbpms2b*^{chb4} by fluorescent PCR and DNA-fragment analysis are shown (Table S5). The wild-
137 type alleles produce amplicons of 97 base pairs (bp)(*rbpms2a*) and 76bp (*rbpms2b*), whereas
138 the mutant alleles produce amplicons of 83bp (*rbpms2a*^{chb3}) and 74bp (*rbpms2b*^{chb4}).
139

140 **hiPSC maintenance and genome editing**

141 All hiPSC lines were maintained at 37°C, 5% CO_2 in Essential 8 medium (Cat. # A1517001,
142 Thermo Fisher Scientific) and passaged every 3 – 4 days using Versene (Cat. # 15040066,
143 Thermo Fisher Scientific). Culture dishes were pre-coated with 0.5% GelTrex matrix solution
144 (Cat. # A1413302, Thermo Fisher Scientific). CRISPR/Cas9 genome editing was performed to
145 create isogenic lines. Briefly, guide RNA for *RBPMS2* (sequence 5'-
146 GTCTTGCAGTGAGCTTGATC-3') was synthesized using the T7 MegaShortScript transcription
147 kit (Thermo Fisher Scientific). We previously described methods [28] to generate a doxycycline -
148 inducible Cas9 line in the WTC-11 iPSC background (Coriell Institute). Targeted integration of
149 Cas9 into the AAVS1 locus was performed using Addgene plasmids #73500 and #48139. This
150 WTC-11 AAVS1$^{Cas9/+}$ hiPSC line was treated with doxycycline (2μg/ml) for 16 hours prior to
151 transfection to induce expression of an NLS-SpCas9 fusion protein. After induction,
152 approximately 0.5 x10^6 cells were transfected with 10μg guide RNA using an Amaxa
153 nucleofector (Lonza Technologies). Cells were seeded at a low density to pick single clones.
154 Positive clones were confirmed by Sanger and amplicon sequencing. Stem cell marker
155 expression was validated in isolated cell lines by flow cytometry using anti-SSEA4-FITC (Cat. #
156 130-098-371, Miltenyi Biotec).
157

158 **RESULTS**

159 *Differential expression analysis of FACS-purified zebrafish anterior lateral plate mesodermal*
160 *cells identifies cardiomyocyte-restricted expression of rbpms2a and rbpms2b*

161 Lineage-restricted genes often perform specialized and essential functions in the
162 development, maintenance, or function of the populations they mark. To generate a candidate
163 list of zebrafish genes with essential activities in cardiopharyngeal progenitors or embryonic
164 cardiomyocytes, we sought to identify mRNAs with restricted expression to the subset of
165 anterior lateral plate mesodermal (ALPM) cells marked by the *nkx2.5:ZsYellow* transgene. This
166 population contains cardiopharyngeal progenitors for multiple cell types including second heart
167 field-derived ventricular cardiomyocytes, three outflow tract (OFT) lineages, a subset of
168 pharyngeal muscles, and endothelium of the pharyngeal arch arteries [20,29–32]. It also contains
169 early-differentiating ventricular cardiomyocytes derived from the first heart field [29,31,32].

170 To isolate ALPM cells labeled with the transgene, *Tg(nkx2.5:ZsYellow)* embryos were
171 dissociated to single cells at a developmental stage when ZsYellow fluorescence is restricted to
172 the ALPM [14-16 somites stage (ss); Fig. 1A]. Dissociated cells were separated by FACS into
173 ZsYellow-positive and ZsYellow-negative subpopulations before being subjected to RNA-
174 sequencing and differential expression analysis (Fig 1A; Fig S1A-C). From this, we identified
175 1848 protein-coding RNAs significantly enriched in the ZsYellow-positive population [fold
176 change (FC)>1.5; adjusted p-value<0.05; Fig. 1A; Fig. S1D; Table S1]. Among them were
177 several previously characterized lateral plate mesodermal markers that encode transcription
178 factors essential for vertebrate cardiopharyngeal development including *nkx2.5*, *hand2*,
179 *gata4/5/6*, *mef2ca/b*, *tbx1/5a/20*, *isl1*, and *fgf8a/10a/10b* (Fig. S1D; Table S1). Due to the
180 presence of early-differentiating cardiomyocytes in the ZsYellow-positive population, we also
181 identified numerous genes encoding sarcomere components [*cmlc1*, *myl7* (*cmlc2*), *myh7*
182 (*vmhc*), *myh6* (*amhc*), *acta1b*, *actc1a*, *actn2b*, *tnni1b*, *tnnt2a, tnnc1a, tpm4a, ttn.2*], calcium
183 handling proteins [*slc8a1a* (*ncx1*), *ryr2b, atp2a2a (serca2)*] and other factors expressed
184 preferentially in cardiomyocytes (*cx36.7*, *nppa/al/b*; Fig. S1D; Table S1). Not surprisingly, gene

185 ontology (GO) term enrichment analysis uncovered overrepresentation of biological process
186 terms “heart development”, “angiogenesis”, “heart contraction”, “actin cytoskeletal organization”,
187 and “sarcomere organization” in the ALPM-enriched gene set (Fig. S1E, see Table S1 for
188 complete GO term analysis). The successful identification of ALPM markers with well-
189 documented and indispensable roles in cardiopharyngeal progenitors or cardiomyocytes
190 suggests that novel molecular activities of equal importance are likely to be among the
191 uncharacterized ALPM-restricted genes.

192 Transcripts encoding RNA binding protein with multiple splicing (variants) 2a (Rbpms2a)
193 and Rbpms2b were enriched 14- and 5-fold, respectively, in the ZsYellow-positive population
194 (Fig. S1D; Table S1), suggesting that these RNA-recognition motif (RRM)-containing proteins
195 localize to the ALPM. Classified as ohnologs, *rbpms2a* and *rbpms2b* encode proteins that are
196 92% identical and perform redundant functions in oocyte differentiation [33]. Across the full-length
197 amino acid sequences, Rbpms2a and Rbpms2b share greater than 81% identity with human
198 RBPMS2 (Fig. S2A,B). The shared identity exceeds 92% in the RRMs (Fig. S2A,B). Such a high
199 degree of sequence conservation suggests that the molecular function of RBPMS2 proteins and
200 the properties of their binding site sequences are also likely to be conserved across evolution.

201 The founding member of the *RBPMS2* gene family, originally termed *hermes*, was
202 discovered in a differential expression screen designed to identify heart-specific transcripts in
203 *Xenopus* [34,35]. In situ hybridization revealed that *RBPMS2* localizes to the lateral plate
204 mesoderm and embryonic myocardium in both amphibian and avian species [34,36]. Hearts of
205 embryonic zebrafish were also recently reported to express *rbpms2a* and *rbpms2b* [33]. Despite
206 the high degree of amino-acid sequence conservation and consistent myocardial-restricted
207 expression pattern across vertebrates, *RBPMS2* has yet to be implicated in any aspect of
208 myocardial biology through genetic loss-of-function studies.

209 To validate the predicted ALPM localization of *rbpms2a* and *rbpms2b,* we performed in
210 situ hybridization for both genes at the same developmental stage used for profiling

211 *nkx2.5:ZsYellow*-positive ALPM cells (16 ss; Fig. S1). As anticipated, both transcripts localized
212 bilaterally to the ALPM (Fig. 1B,E) in a pattern mirroring early-differentiating cardiomyocytes in
213 at this stage [37]. Later-stage analysis revealed *rbpms2a* and *rbpms2b* expression in the heart
214 tube at 24-28 hours post fertilization (hpf; Fig. 1C,F; Fig. S3A,C) and in the atrium and ventricle
215 of the two-chambered heart at 48 hpf (Fig. 1D,G; Fig. S3B,D). Consistent with previous reports
216 [33,38], extra-cardiac expression was observed in the pronephric duct and retina (Fig. S3A-D)
217 To investigate the lineage specificity and subcellular localization of Rbpms2a and
218 Rbpms2b in the zebrafish heart, we immunostained wild-type embryos with a monoclonal
219 antibody raised against human RBPMS2, which cross reacts with zebrafish Rbpms2 (see
220 below). Consistent with the distribution of *rbpms2a/b* transcripts, Rbpms2 protein was detected
221 in the heart tube (Fig. 1H,I; Fig. S3E,F), two chambered heart (Fig. 1J,K; Fig. S3G), pronephric
222 duct (Fig. S3E-G) and retina (Fig. S3F,G). Double-immunostaining for Rbpms2 and the
223 myocardial marker cardiac Troponin T (CT3) revealed that Rbpms2 expression localizes to the
224 myocardium at all stages analyzed (Fig. 1H',I',J',K'). Weak expression of Rbpms2 was also
225 evident by 72 hpf in the OFT (i.e. bulbous arteriosus; Fig. 1K,K'). Examination of single optical
226 sections through the ventricular wall, which showed nuclear Rbpms2 signals surrounded by
227 Troponin T-positive cytoplasm, confirmed myocardial localization of Rbpms2, (Fig. 1L-L''').
228 Adjacent endocardial cells were devoid of Rbpms2 signals, which highlights the myocardial-
229 specific nature of Rbpms2 expression (Fig. 1L-L'''). The subcellular distribution of Rbpms2
230 appeared variable, ranging from a nucleocytoplasmic distribution to exclusively nuclear (Fig.
231 1H,I,J,K), but the significance of this observation is unknown. Lastly, we documented Rbpms2
232 expression in the nuclei and cytoplasm of cardiomyocytes in hearts from adult zebrafish (Fig.
233 1M,M'), suggesting that Rbpms2 functions in the myocardium continuously throughout the
234 lifespan of zebrafish rather than transiently during embryogenesis.
235
236 *Generation of Rbpms2-null zebrafish*

237 To discover if *rbpms2a* and *rbpms2b* are required for myocardial development or
238 function, we created mutant alleles of both genes using transcription activator-like effector
239 nucleases (TALENs) [24]. TALEN pairs were designed to target DNA sequences encoding N-
240 terminal regions of the RRM domains (Fig. S4A,B). We isolated the mutant alleles *rbpms2a*^{chb3}
241 and *rbpms2b*^{chb4}, which carry frame-shifting deletions and pre-mature stop codons that truncate
242 the proteins by >80% (Fig. 2A,B; Fig. S4A,B). The truncations also remove 82% of the RRMs,
243 suggesting that the RNA-binding activities of the mutant proteins are abolished or significantly
244 compromised. As a result, both alleles are likely to be null. Animals homozygous for either
245 *rbpms2a*^{chb3} or *rbpms2b*^{chb4} are grossly indistinguishable from siblings during all life stages,
246 which is consistent with a previous study that independently generated mutant alleles of
247 *rbpms2a* and *rbpms2b* [33].
248 To determine if *rbpms2a* and *rbpms2b* perform redundant functions in the heart, we
249 generated and monitored double homozygous embryos [i.e. *rbpms2a*$^{chb3/chb3}$*; rbpms2b*$^{chb4/chb4}$
250 animals, referred to hereafter as *rbpms2*-null, double-mutant, or double-knockout (DKO)
251 embryos or animals] for cardiac defects. DKO animals are grossly indistinguishable from control
252 siblings for the first ~30 hours of life. By ~33 hpf, they develop a characteristic indentation of the
253 yolk, which is indicative of mild pericardial edema (Fig. S4C,D). At this stage, double-mutants
254 are delayed in initiating blood flow even though peristalsis of the heart tube is readily evident. By
255 72 hpf, pericardial edema becomes progressively more severe (Fig. 2C,D), suggesting that
256 *rbpms2*-null animals suffer from a cardiac malformation or ongoing functional deficit.
257 Western blotting and whole mount immunostaining revealed that the zebrafish epitopes
258 recognized by the anti-human RBPMS2 antibody are completely absent in double mutants (Fig.
259 2E-G), demonstrating that the antibody cross reacts with zebrafish Rbpms2. It also suggests
260 that the mutant mRNAs or proteins are unstable, further suggesting that *rbpms2a*^{chb3} and
261 *rbpms2b*^{chb4} are bona fide null alleles.

262 To assess double-mutant viability, we monitored the survival of control-sibling and DKO
263 animals from embryonic stages to adulthood. Over 50% of *rbpms2*-null animals died by two
264 weeks of age (Fig. 2H). Eighty five percent of animals perished by 60 days post fertilization
265 (dpf), and the remaining small percentage of animals did not survive beyond 6 months post
266 fertilization. At all ages, death was generally accompanied by progressively severe pericardial
267 edema, suggesting a cardiac origin. Together, these data reveal that *rbpms2a* and *rbpms2b*
268 ohnologues perform redundant functions that are essential to zebrafish survival.
269

270 *rbpms2a and rbpms2b are required for chamber expansion during ventricular filling*

271 To evaluate DKO embryos for structural heart disease, we examined hearts in 48 hpf
272 control-sibling and *rbpms2*-null animals carrying the *myl7:GFP* transgene, which labels the
273 entire myocardium with GFP. Although the two-chambered heart in double mutants displayed
274 normal left-right patterning, the ventricle was displaced anteriorly relative to the atrium (Fig.
275 2I,J), likely reflecting stretching at the cardiac poles caused by pericardial edema. Atrial size
276 was not obviously altered in *rbpms2*-null animals, but mutant ventricles appeared smaller (Fig.
277 1I,J). To determine if this might reflect a diminished ventricular cardiomyocyte number, we
278 quantified cardiomyocytes in control-sibling and *rbpms2*-null animals carrying the *myl7:nucGFP*
279 transgene, which labels cardiomyocyte nuclei with GFP (Fig. 2K,L). From this, we learned that
280 ventricular, as well as atrial, cardiomyocyte numbers were unaltered in double mutants (Fig. 2K-
281 M; Fig. S5A), demonstrating that any deviations in chamber size are not attributable to altered
282 myocardial cell content. It also suggests that *rbpms2a* and *rbpms2b* are dispensable for
283 myocardial differentiation from the first and second heart fields, which is the principal method by
284 which cardiomyocytes are produced before 48 hpf [20,39–41]. These data demonstrate that early
285 cardiac morphogenesis is largely unperturbed in double mutant animals, with the only apparent
286 anatomical abnormality being a reduction in ventricular size.

287 To characterize potential functional defects in *rbpms2*-null hearts, we measured ejection
288 fraction and cardiac output in 48 hpf animals using our previously described Cardiac Functional
289 Imaging Network [CFIN; [42]]. To that end, we captured Z-stack dynamic images of GFP+ hearts
290 over several cardiac cycles in control-sibling and DKO *myl7:GFP* transgenic embryos using light
291 sheet fluorescence microscopy. CFIN extracted chamber volumes and identified the maximum
292 and minimum ventricular volumes throughout the cardiac cycle, referred to as end-diastolic
293 volume (EDV; maximum volume during cardiac relaxation) and end-systolic volume (ESV;
294 minimum volume during cardiac contraction), respectively. Whereas the ESV was unchanged in
295 DKO animals, the EDV was significantly reduced (Fig. 2N-R), demonstrating that the ventricle
296 fails to expand during the relaxation phase of the cardiac cycle. As a result, three indices of
297 ventricular function, all of which are calculated from EDV and ESV, were significantly reduced.
298 These include stroke volume (SV), the volume of blood expelled by the ventricle per beat
299 (SV=EDV-ESV), ejection fraction, the percentage of blood expelled by the ventricle per beat
300 (EF=SV/EDV), and cardiac output, the total volume of blood expelled by the ventricle per minute
301 (SV*heart rate) (Fig. 2R). Heart rate was unchanged in the mutant (Fig. 2R). CFIN analysis also
302 revealed an increase in atrial volume (Fig. S5B), which was not grossly obvious after fixation
303 (Fig. 2I,J) and is a common secondary consequence of impaired ventricular function [43–45]. These
304 data demonstrate that *rbpms2a* and *rbpms2b* are required for ventricular function in the
305 zebrafish embryo. Further, this requirement likely extends into adulthood because the longest-
306 living double-mutant animals exhibited several signs of heart failure such as stunted growth,
307 pericardial edema, and cardiac pathologies including compact, fibrotic ventricles and massively
308 enlarged atria (Fig. S6A-E).
309
310 *Identification of differential alternative splicing events in rbpms2-null zebrafish*
311 To identify transcriptomic abnormalities in the hearts of *rbpms2*-null embryos, we
312 performed bulk RNA-sequencing and differential expression analysis on control-sibling and

313 *rbpms2*-null animals at 33 hpf, the earliest developmental stage when DKO animals are
314 distinguishable by morphology (Fig. S4C,D). We reasoned that early-stage analysis would
315 maximize the chances of highlighting primary molecular defects without interference by
316 secondary responses to cardiac dysfunction. Importantly, we confirmed that the primitive
317 ventricle in 33 hpf *rbpms2*-null animals exhibits a functional deficit by documenting reduced
318 myocardial wall movement at the arterial pole of the heart tube (Fig. S7A). We also confirmed
319 that total cardiomyocyte numbers are unaltered at 33 hpf in double mutants (Fig. S7B), reducing
320 the chances that any transcriptomic abnormalities would be attributable to altered cellular
321 composition. Lastly, we profiled whole embryos, instead of purified hearts, because effective
322 protocols for isolating hearts or cardiomyocytes at this early stage do not currently exist.
323 Nonetheless, because *rbpms2a* and *rbpms2b* are expressed with exquisite specificity in the
324 heart, retina and pronephric duct (Fig. S3F), we anticipated that the transcriptional changes
325 occurring in the myocardium would be a discernable subset of those occurring in the whole
326 animal.
327 While RNA-sequencing and gene-level differential expression analysis highlighted only 2
328 downregulated transcripts in *rbpms2*-null animals (|FC|>1.5; p-adj<0.05; Table S2; Figure S8A),
329 isoform-level differential expression analysis yielded 78 downregulated and 74 upregulated
330 transcripts (|FC|>1.5; p-adj<0.05; Table S3; Fig. S8B). GO term analysis did not identify
331 overrepresentation of any terms in either gene set [False Discovery Fate (FDR)<0.05].
332 However, among the downregulated transcripts, there were three well-characterized myocardial
333 genes including *phospholamban* (*pln*; FC=-43.00; p-adj=1.53E-09), *atrial myosin heavy chain 6*
334 (*myh6*; FC=-2.17; p-adj=1.52E-11), and *natriuretic peptide precursor a* (*nppa*; FC=-1.57; p-
335 adj=0.019; Fig. S8B; Table S2). We confirmed downregulation of *nppa* by reverse-transcription
336 quantitative PCR (RT-qPCR) at 33hpf (Fig. S7C). However, this reduction was short lived
337 because two subsequent developmental stages showed increased *nppa* expression (Fig. S7C),
338 which is characteristic behavior for *nppa* in response to cardiac stress [46]. RT-qPCR analysis of

339 *myh6* revealed a downward trending but statistically insignificant change in double mutants (Fig.
340 S7D). Ultimately, downregulation of either gene is unlikely to explain the ventricular phenotype
341 in *rbpms2*-null mutants because *nppa*-null zebrafish do not exhibit any gross cardiac defects [47]
342 and the primary defect in *myh6*-deficient animals is a silent atrium [48].
343 Of the two *pln* genes in the zebrafish genome (GRCZ11), *si:ch211-270g19.5*
344 (ENSDARG00000097256) and *pln* (ENSDARG00000069404), the latter is alternatively spliced
345 according to publicly available cDNA sequencing data. Interestingly, only one of the
346 alternatively-spliced *pln* isoforms (ENSDART00000141159; *pln-203*) was found to be
347 downregulated in *rbpms2*-null animals (FC=-43.00; p-adj1.53E-09; Fig. S8B; Table S2). The
348 other *pln* transcript (ENSDART00000133911**;** *pln-202***)** was unchanged (FC=1.37; p-adj>0.99;
349 Table S2), which highlighted the possibility that Rbpms2 functions in the zebrafish myocardium
350 to regulate alternative splicing, a molecular function previously ascribed to the closely related
351 RBPMS protein [49], but not to RBPMS2 itself [35].
352 To investigate this possibility directly, we performed replicate multivariate analysis of
353 transcript splicing (rMATS) [50] on the same RNA-sequencing dataset and identified 150
354 differential alternative splicing events (ASEs) in *rbpms2*-null animals (0 uncalled replicates;
355 FDR<0.01; |Incleveldifference|>0.1; Fig. 3A,B; Table S3). The most common ASE was skipped
356 exon (SE), representing over 40% of the total ASEs, followed by alternative 3' splice site (A3SS,
357 23%), alternative 5' splice site (A5SS, 21%), mutually exclusive exons (MXE, 10%), and
358 retained intron (RI, 6%) (Fig 3A,C). Gene ontology (GO) term enrichment analysis did not
359 identify overrepresentation of any terms among the differentially spliced genes. However, a
360 limited number of myocardial genes were found to be differentially spliced in *rbpms2*-null
361 animals including *myosin binding protein C3* (*mybpc3*) and *myomesin 2a* (*myom2a*), both of
362 which encode sarcomere components [51–54], and *solute carrier family 8 member 1a* [*slc8a1a*;
363 also termed the *sodium calcium exchanger 1* (*ncx1*)] which encodes a plasma membrane

364 transporter responsible for extruding calcium from cardiomyocytes during cardiac relaxation
365 [55,56].
366 In the case of *mybpc3*, exons 2 and exons 10 were identified as cassette exons whose
367 inclusion levels (Inclevels) in mature *mybpc3* transcripts were found to be significantly lower in
368 *rbpms2*-null animals (exon2 Inclevel=0.031; exon 10 Inclevel=0.057) when compared to those in
369 control siblings (exon2 Inclevel=0.557; exon10 Inclevel=0.296; exon 2 Incleveldifference=0.526,
370 FDR=4.77E-40; exon 10 Incleveldifference=0.24, FDR=2.38E-21; Fig. 3B; Fig.4A; Table S4).
371 The same was true for exon 16 of *myom2a* (control Inclevel=1, DKO Inclevel=0,
372 Incleveldifference=1, FDR 2.74E-20; Fig. 3B; Fig.4A; Table S4) and exon 5 of *slc8a1a* (control
373 Inclevel=1, DKO Inclevel=0.37, Incleveldifference=0.629, FDR=4.92E-14; Fig. 3B; Fig.4A; Table
374 S4). In all cases, exon inclusion was higher in in control siblings, which means that these exon
375 sequences were significantly reduced or absent in *rbpms2*-null animals.
376 Despite supporting evidence from differential isoform expression analysis (Fig. S8B;
377 Table S2), rMATS did not identify alternative splicing of *pln*, likely because it involves a terminal
378 exon (Fig. 4A), which rMATS is not designed to evaluate (Fig. 3A). Therefore, we employed the
379 mixture of isoforms (MISO) algorithm [57] to evaluate alternative splicing of *pln* in *rbpms2*-null
380 animals and found strong statistical evidence that the exon 3-containing *pln*-203 isoform
381 (ENSDART00000141159) is uniquely reduced in mutant animals. Specifically, the Bayes factor
382 was largely above the accepted cutoff of 5 for differences in ENSDART00000141159 versus
383 ENSDART00000133911 usage in WT and double-mutant animals across all five replicate pairs
384 (Table S5), which is strongly suggestive of differential alternative splicing. This conclusion was
385 also supported by genotype-specific differences in read densities across the locus (Fig. S9).
386 Collectively, these data demonstrate that *rbpms2*-null embryos display abnormal splicing of
387 genes that are essential to cardiac function.
388
389 *Validation of differential alternative splicing events in rbpms2-null zebrafish*

390 Next, we used splicing-sensitive RT-qPCR to validate differential alternative splicing of
391 *mybpc3*, *myom2a*, *slc8a1*, and *pln* in *rbpms2*-null animals at 48 hpf (Fig. 4A). To that end, we
392 designed two primer pairs for each transcript. One was designed to measure relative "total
393 transcript" levels between sibling control and *rbpms2*-null animals, independent of the
394 alternatively spliced exon. The other was designed to quantify relative "isoform-specific" levels
395 by having one of the primer-binding sites contained within the exon of reduced inclusion
396 according to rMATS or MISO (Fig. 4A). For all four genes, total transcript levels were not
397 significantly altered in *rbpms*2-null animals (Fig. 4B). However, the specific exon-containing
398 isoforms were reduced by at least 50% in all cases, and by greater than 95% in three cases,
399 indicative of almost-complete exon exclusion (Fig. 4C). Taken together, these data provide
400 strong evidence that Rbpms2 activity promotes the inclusion of specific exons into mature
401 cardiac transcripts. Importantly, we verified that *mybpc3* and *pln* are also abnormally spliced
402 earlier in development (33 hpf), when signs of cardiac distress first become visible in double
403 mutants, reducing the likelihood that abnormal splicing is a secondary consequence of cardiac
404 dysfunction (Fig. S7E,F).
405 To confirm that the DKO splicing abnormalities localize to the myocardium, we
406 performed splicing-sensitive in situ hybridization analysis for two genes, *mybpc3* and *pln*, with
407 *rbpms2*-dependent exons large enough to generate effective exon-specific anti-sense
408 riboprobes (i.e. exon 2 of *mybpc3* and exon 3 of *pln*; Fig. 4A). In a strategy analogous to the
409 splicing-sensitive qPCR, we designed a pair of riboprobes for each gene. One probe detected
410 the total transcript pools of *mybpc3* or *pln*, independent of the alternatively spliced exons
411 ("Total-transcript" in situ hybridization). The other probe detected the alternatively spliced exon
412 sequences exclusively. In control-sibling animals at 33 hpf, total *mybpc3* transcripts were
413 localized to both cardiac and skeletal muscle (Fig. 4D,D'), and total *pln* transcripts were
414 detected exclusively in the heart (Fig. 4H,H'). These expression patterns were unaffected by the
415 loss of *rbpms2* (Fig. 4E,E',I,I'), which is consistent with the total transcript qPCR analysis (Fig.

416 4B). Isoform-specific in situ hybridization analysis revealed expression of the *rbpms2*-dependent
417 *mybpc3* and *pln* exons exclusively in the hearts of control-sibling animals (Fig. 4F,F',J,J').
418 Consistent with the isoform-specific qPCR analysis (Fig. 4C), double-mutant animals were
419 completely devoid of these exon sequences (Fig. 4G,G',K,K'). Taken together, these data
420 implicate *rbpms2* as a positive regulator of exon inclusion in the zebrafish embryonic
421 myocardium.

422 For those alternative splicing events validated by qPCR or in situ hybridization (*mybpc3*,
423 *myom2a*, *pln*, and *slc8a1a*), exon exclusion in mutant hearts maintains the open reading frame,
424 indicating that the hearts of mutant animals express proteins lacking amino acid sequences
425 encoded by the alternatively spliced exons (Fig. 4E,E',G,G'I,I',K,K'). In the case of *mybpc3,*
426 exon 2 encodes a domain termed C0, which is contained exclusively within the cardiac isoform
427 of Myosin Binding Protein C in higher vertebrates (MYBPC3) but is absent from the skeletal
428 muscle isoform [MYBPC2; [58]]. Similarly, *mybpc3*'s exon 10 encodes cardiac-specific amino
429 acids that become phosphorylated by protein kinase A (PKA) in response to β-adrenergic
430 signaling [59,60]. For Myom2a, the short stretch of amino acids that disappears in DKO animals is
431 of unknown function. For *pln*, excluding exon 3 shortens the protein by 5 amino acids on the C-
432 terminus, which has been shown to increase SERCA inhibitory activity *in vitro* [6]. Lastly, the
433 *slc8a1a* exon with reduced inclusion in DKO animals is one of six conserved exons that are
434 alternatively spliced in higher vertebrates to control the Ca2+ sensitivity of the transporter [61,62].
435

436 *Zebrafish rbpms2-null ventricular cardiomyocytes exhibit myofibrillar disarray and calcium*
437 *handling defects*

438 Because Mybpc3 and Myom2a are sarcomere components, we evaluated 48 hpf
439 control-sibling and double-mutant hearts for myofibrillar defects after immunostaining with
440 antibodies that recognize thin filaments, thick filaments, or Z-disks. For all epitopes, prominent
441 striations were apparent in control-sibling animals reflecting the tandem arrays of sarcomeres

442 composing myofibrils, which themselves are transversely aligned and bundled near the cell
443 cortices (Fig. 5A,A',C-C",E). By contrast, despite the readily-evident detection of epitopes in
444 DKO hearts, striations were significantly reduced or absent because the myofibrils were in a
445 state of disarray (Fig. 5B,B',D-D",F). We confirmed that myofibril disarray was also present in
446 ventricular cardiomyocytes of double mutant animals at an earlier developmental stage of 33 hpf
447 (Fig. S7G-H'). Lastly, this defect is specific to ventricular cardiomyocytes because myofibril
448 organization in atrial cardiomyocytes of control and DKO embryos was grossly indistinguishable
449 (Fig. S7I-J'). Taken together, these data demonstrate that Rbpms2 activity is required for
450 establishing or maintaining the three-dimensional architecture of myofibrils in ventricular
451 cardiomyocytes of the zebrafish embryo.

452 Lastly, because *pln* and *slc8a1a* regulate calcium handing in cardiomyocytes [56,63–65], we
453 evaluated *rbpms2*-null hearts for abnormalities in the amplitude or duration of cytosolic calcium
454 transients, which stimulate cardiomyocyte contraction. To that end, control-sibling and *rbpms2*-
455 null hearts at 48 hpf were explanted and loaded with the dual-wavelength calcium-sensitive dye
456 Fura-2. High-speed imaging was performed to obtain a ratiometric indicator of fluctuating
457 calcium in cardiomyocytes over several cardiac cycles [66]. From this, we measured the duration
458 and amplitude of the calcium transients in the atrium and ventricle of control-sibling and *rbpms2*-
459 null hearts. Whereas these values were not significantly different in the atrium of double mutant
460 hearts (Fig. 6A,B,D-F,H), both the duration and amplitude of the calcium transients in double
461 mutant ventricles were reduced in the mutant ventricle (Fig. 6A-C; E-G), demonstrating that
462 Rbpms2 is indispensable for the regulation of calcium handling in ventricular cardiomyocytes of
463 the zebrafish embryo.

464

465 *Human RBPMS2-null cardiomyocytes exhibit myofibrillar disarray and calcium handling defects*

466 To determine if the cellular function of *RBPMS2* is conserved in human cardiomyocytes,
467 we targeted *RBPMS2* in human induced pluripotent stem cells (hiPSCs) using CRISPR/Cas9-

468 mediated genome editing and analyzed phenotypes that arose following differentiation into
469 hiPSC-derived cardiomyocytes (hiPSC-CMs). We targeted the DNA sequence encoding
470 RBPMS2's RNA recognition motif and isolated a clone with a biallelic 2 base-pair deletion (Fig.
471 S10A; *ΔRBPMS*), which truncates both the protein and the RRM by ~70% due to a premature
472 stop codon (Fig. 7A; Fig. S10B). Quantitative RT-PCR analysis revealed a significant 82%
473 reduction in *RBPMS2* transcripts in *ΔRBPMS* hiPSCs (Fig. 7B) and hiPSC-CMs (Fig. 7C),
474 suggesting that the mutant transcripts are susceptible to non-sense mediated decay. This
475 observation, in combination with the large size of the C-terminal truncation (Fig. 7A) strongly
476 suggest that *ΔRBPMS2* cells are null for *RBPMS2*.

477 To determine if *RBPMS2*-null human cardiomyocytes exhibit cellular phenotypes similar
478 to those observed in ventricular cardiomyocytes from *rbpms2*-null zebrafish (Fig. 5A-F), we
479 analyzed myofibril structure in control-parental and *ΔRBPMS2* hiPSC-CMs by double
480 immunostaining with antibodies that detect thin filaments or Z-disks. The hallmark striations
481 created by thin filaments, which were readily apparent in control cells (Fig. 7D,E,G), were
482 almost completely absent in *ΔRBPMS2* hiPSC-CMs (Fig. 7H,I,K). Moreover, whereas the Z-
483 disks in control cardiomyocytes were prominent, well defined and arrayed in parallel (Fig.
484 7D,F,G), those in *ΔRBPMS2* hiPSC-CMs were smaller, punctate, and disorganized (Fig.
485 7H,J,K). Taken together, these data uncover a conserved role for RBPMS2 in establishing or
486 maintaining myofibril organization in human cardiomyocytes.

487 Lastly, we evaluated control-parental and *ΔRBPMS2* hiPSC-CMs for defects in calcium
488 handling. hiPSC-CMs cells were loaded with the calcium-sensitive dye Fluo-4, paced at 1Hz
489 and imaged by line scanning confocal microscopy to capture intracellular Ca2+ dynamics (Fig.
490 7L,M). Similar to ventricular cardiomyocytes from *rbpms2*-null zebrafish, *ΔRBPMS2* hiPSC-CMs
491 exhibited significant decreases in Ca2+-transient amplitude (Fig. 7N) and transient duration
492 (Fig. 7O,P). These phenotypes were accompanied by decreases in time-to-peak (Fig. 7Q) and

493 maximum upstroke velocity (Fig. 7R). Lastly, without pacing, *ΔRBPMS2* hiPSC-CMs contracted
494 at a lower spontaneous beat frequency (Fig. 7S). These data demonstrate that human
495 cardiomyocytes rely on RBPMS2 function for optimal calcium handling. Taken together, the
496 overlap in sarcomere and calcium handling phenotypes observed between *Rbpms2*-null
497 zebrafish and *ΔRBPMS2* hiPSC-CMs suggest that the cellular function(s) of this myocardial
498 RNA-binding protein is conserved in human cardiomyocytes.
499

500 **DISCUSSION**

501 Our study identifies Rbpms2 proteins as critical RNA splicing factors that regulate tissue-
502 specific isoform expression within the ventricular myocardium. Specifically, we show that
503 zebrafish Rbpms2a and Rbpms2b are redundantly required for ventricular form and function in
504 embryonic zebrafish. We then show that Rbpms2 proteins function to promote the generation of
505 distinct isoforms within the heart, including a previously undocumented cardiac-specific isoform
506 of *mybpc3*. Further, we found that *rbpms2*-null hearts have disorganized sarcomeres and
507 disrupted calcium handling, which is phenotypically consistent with the broad classes of
508 alternatively spliced transcripts identified by our RNA-seq. Lastly, we discovered that RBPMS2-
509 deficient human iPSC-CMs exhibit defects in sarcomere structure and calcium handling that are
510 strikingly similar to what we observed in zebrafish ventricles.

511 Our characterization of Rbpms2 provides further evidence that RNA splicing within the
512 heart may be a much more pervasive and physiologically important mode of gene regulation
513 than previously appreciated. While our results reveal a clear connection between Rbpms2 and
514 RNA splicing, these proteins may function in additional capacities within tissues outside the
515 heart. Previous reports in zebrafish have shown that Rbpms2 proteins contribute to the
516 establishment of oocyte polarity and development by influencing the localization of RNAs such
517 as *bucky ball* (*buc*) to the Balbiani body[33,67,68]. Further research in xenopus and chicken have

518 described similar roles for Rbpms2 in RNA stability and localization within intestinal smooth
519 muscle, kidney cells, and retinal ganglion cells[38,69,70]. Interestingly, the localization of Rbpms2 to
520 stress granules has been observed in several of these models[69,71], indicating that this function
521 may be conserved in multiple tissues. It will be important to determine if RBPMS2 functions in
522 this capacity within the heart, or whether this is a tissue-specific function that is restricted to
523 other RBPMS2-positive organs such as the eye and nephron.

524 Even though we found that Rbpms2 regulates the splicing of genes whose orthologs are
525 known to cause cardiomyopathy, it is unclear whether mutations in RBPMS2 segregate with
526 human disease. Our data therefore warrants a careful re-evaluation of existing GWAS datasets
527 and provides new incentives to examine the RBPMS2 locus in CHD patients. However, given
528 the severity of cardiac phenotypes observed in our loss-of-function experiments, it remains
529 possible that embryonic lethality may confound GWAS results. Additionally, the upstream
530 regulators of Rbpms2 remain unknown. Further studies will be necessary to identify these
531 upstream factors in order to determine if they contribute to disease states through a more subtle
532 modulation of Rbpms2 function. Given that Rbpms2 is itself alternatively spliced in vertebrates,
533 it is also possible that its function may be regulated by yet another upstream splicing factor.
534 Collectively these studies will evaluate RBPMS2 function within the broader context of human
535 cardiomyopathy and heart failure.

536

537 **ACKNOWLEDGEMENTS**

538 Fluorescence activated cell sorting was performed at the Harvard Stem Cell Institute-Center for
539 Regenerative Medicine Flow Cytometry Core. Customized TALENs were generated by the
540 Broad Institute Genetic Perturbation Platform (Director: John Doench, PhD). Library preparation,
541 RNA-sequencing, and bioinformatics analyses were performed at the MIT BioMicroCenter
542 (Director: Stuart Levine, PhD). Ryan Abo of the MIT BioMicroCenter provided assistance with
543 bioinformatics analysis. Sanger sequencing and DNA fragment analysis were performed at the

Massachusetts General Hospital Computational and Integrative Biology DNA Core (Director: Amy Avery).

FUNDING

AAA was supported by an American Heart Association Postdoctoral Fellowship (20POST35110027). AAA and AS were supported by a National Institutes of Health (NIH) training grant awarded to Massachusetts General Hospital (MGH) (T32HL007208; PI: A. Rosenzweig). The Burns Laboratory was supported by NIH grants 7R01HL139806 (formerly 1R01HL139806) and 7R35HL135831 (formerly 1R35H135831) to CGB and CEB, respectively, by awards from the Executive Committee on Research at MGH to CGB, and by Department of Defense Peer-Reviewed Medical Research Program (PRMRP) grant PR190628 to CEB. CEB was a d'Arbelhoff MGH Research Scholar. CGB was a Hassenfeld Cardiovascular Scholar at MGH. The Burns Laboratory was supported, in part, by funds from the Boston Children's Hospital Department of Cardiology.

MT was supported by an NIH training grant awarded to Boston Children's Hospital (T32HL007572; PI: W. Pu). The bioinformatics analysis was supported in part by the Koch Institute Support (core) Grant P30-CA14051 from the National Cancer Institute.

COMPETING INTERESTS

The authors declare no competing interests.

REFERENCES

1. Virani SS, Alonso A, Aparicio HJ, Benjamin EJ, Bittencourt MS, Callaway CW, Carson AP, Chamberlain AM, Cheng S, Delling FN, Elkind MSV, Evenson KR, Ferguson JF, Gupta DK, Khan SS, et al. Heart Disease and Stroke Statistics—2021 Update: A Report From the American Heart Association. *Circulation*. 2021:CIR0000000000000950.

571 2. Skrzynia C, Berg J, Willis M, Jensen B. Genetics and Heart Failure: A Concise Guide for the Clinician.
572 *Current Cardiology Reviews*. 2014;11(1):10–17.

573 3. Garfinkel AC, Seidman JG, Seidman CE. Genetic Pathogenesis of Hypertrophic and Dilated
574 Cardiomyopathy. *Heart Failure Clinics*. 2018;14(2):139–146.

575 4. Towbin JA, Bowles NE. Genetic abnormalities responsible for dilated cardiomyopathy. *Current*
576 *Cardiology Reports*. 2000;2(5):475–480.

577 5. Towbin JA. Molecular genetics of hypertrophic cardiomyopathy. *Current Cardiology Reports*.
578 2000;2(2):134–140.

579 6. Gorski PA, Ceholski DK, Hajjar RJ. Altered Myocardial Calcium Cycling and Energetics in Heart
580 Failure—A Rational Approach for Disease Treatment. *Cell Metabolism*. 2015;21(2):183–194.

581 7. Hoogenhof MMG van den, Beqqali A, Amin AS, Made I van der, Aufiero S, Khan MAF, Schumacher
582 CA, Jansweijer JA, Spaendonck-Zwarts KY van, Remme CA, Backs J, Verkerk AO, Baartscheer A, Pinto
583 YM, Creemers EE. RBM20 Mutations Induce an Arrhythmogenic Dilated Cardiomyopathy Related to
584 Disturbed Calcium Handling. *Circulation*. 2018;138(13):1330–1342.

585 8. Guo W, Schafer S, Greaser ML, Radke MH, Liss M, Govindarajan T, Maatz H, Schulz H, Li S, Parrish
586 AM, Dauksaite V, Vakeel P, Klaassen S, Gerull B, Thierfelder L, et al. RBM20, a gene for hereditary
587 cardiomyopathy, regulates titin splicing. *Nature Medicine*. 2012;18(5):766–773.

588 9. Maatz H, Jens M, Liss M, Schafer S, Heinig M, Kirchner M, Adami E, Rintisch C, Dauksaite V, Radke
589 MH, Selbach M, Barton PJR, Cook SA, Rajewsky N, Gotthardt M, et al. RNA-binding protein RBM20
590 represses splicing to orchestrate cardiac pre-mRNA processing. *Journal of Clinical Investigation*.
591 2014;124(8):3419–3430.

592 10. LeWinter MM, Granzier HL. Titin Is a Major Human Disease Gene. *Circulation*. 2013;127(8):938–
593 944.

594 11. Haas J, Frese KS, Peil B, Kloos W, Keller A, Nietsch R, Feng Z, Müller S, Kayvanpour E, Vogel B,
595 Sedaghat-Hamedani F, Lim W-K, Zhao X, Fradkin D, Köhler D, et al. Atlas of the clinical genetics of
596 human dilated cardiomyopathy. *European Heart Journal*. 2015;36(18):1123–1135.

597 12. Refaat MM, Lubitz SA, Makino S, Islam Z, Frangiskakis JM, Mehdi H, Gutmann R, Zhang ML,
598 Bloom HL, MacRae CA, Dudley SC, Shalaby AA, Weiss R, McNamara DM, London B, et al. Genetic
599 variation in the alternative splicing regulator RBM20 is associated with dilated cardiomyopathy. *Heart*
600 *Rhythm*. 2012;9(3):390–396.

601 13. Liu J, Kong X, Zhang M, Yang X, Xu X. RNA binding protein 24 deletion disrupts global alternative
602 splicing and causes dilated cardiomyopathy. *Protein & Cell*. 2019;10(6):405–416.

603 14. Gaertner A, Brodehl A, Milting H. Screening for mutations in human cardiomyopathy- is RBM24 a
604 new but rare disease gene? *Protein & Cell*. 2019;10(6):393–394.

605 15. Jin JP, Lin JJ. Isolation and Characterization of cDNA Clones Encoding Embryonic and Adult
606 Isoforms of Rat Cardiac Troponin T. *Journal of Biological Chemistry*. 1989;264(24):14471–14477.

607 16. Farza H, Townsend PJ, Carrier L, Barton PJ, Mesnard L, Bährend E, Forissier J-F, Fiszman M,
608 Yacoub MH, Schwartz K. Genomic Organisation, Alternative Splicing and Polymorphisms of the Human
609 Cardiac Troponin T Gene. *Journal of Molecular and Cellular Cardiology*. 1998;30(6):1247–1253.

610 17. Biesiadecki BJ, Elder BD, Yu Z-B, Jin J-P. Cardiac Troponin T Variants Produced by Aberrant
611 Splicing of Multiple Exons in Animals with High Instances of Dilated Cardiomyopathy*. *Journal of*
612 *Biological Chemistry*. 2002;277(52):50275–50285.

613 18. Niimura H, Bachinski LL, Sangwatanaroj S, Watkins H, Chudley AE, McKenna W, Kristinsson A,
614 Roberts R, Sole M, Maron BJ, Seidman JG, Seidman CE, Thierfelder L, Jarcho JA, Anastasakis A, et al.
615 Mutations in the Gene for Cardiac Myosin-Binding Protein C and Late-Onset Familial Hypertrophic
616 Cardiomyopathy. *The New England Journal of Medicine*. 1998;338(18):1248–1257.

617 19. MacLennan DH, Kranias EG. Phospholamban: a crucial regulator of cardiac contractility. *Nature*
618 *Reviews Molecular Cell Biology*. 2003;4(7):566–577.

619 20. Zhou Y, Cashman TJ, Nevis KR, Obregon P, Carney SA, Liu Y, Gu A, Mosimann C, Sondalle S,
620 Peterson RE, Heideman W, Burns CE, Burns CG. Latent TGF-β binding protein 3 identifies a second
621 heart field in zebrafish. *Nature*. 2011;474(7353):645–648.

622 21. Burns CG, Milan DJ, Grande EJ, Rottbauer W, MacRae CA, Fishman MC. High-throughput assay for
623 small molecules that modulate zebrafish embryonic heart rate. *Nature Chemical Biology*. 2005;1(5):263–
624 264.

625 22. González-Rosa JM, Sharpe M, Field D, Soonpaa MH, Field LJ, Burns CE, Burns CG. Myocardial
626 Polyploidization Creates a Barrier to Heart Regeneration in Zebrafish. *Developmental Cell*.
627 2018;44(4):433-446.e7.

628 23. Lin Y-F, Swinburne I, Yelon D. Multiple influences of blood flow on cardiomyocyte hypertrophy in
629 the embryonic zebrafish heart. *Developmental Biology*. 2012;362(2):242–253.

630 24. Sander JD, Cade L, Khayter C, Reyon D, Peterson RT, Joung JK, Yeh J-RJ. Targeted gene disruption
631 in somatic zebrafish cells using engineered TALENs. *Nature Biotechnology*. 2011;29(8):697–698.

632 25. Ma AC, Lee HB, Clark KJ, Ekker SC. High efficiency In Vivo genome engineering with a simplified
633 15-RVD GoldyTALEN design. Müller F, ed. *PloS one*. 2013;8(5):e65259.

634 26. Sanjana NE, Cong L, Zhou Y, Cunniff MM, Feng G, Zhang F. A transcription activator-like effector
635 toolbox for genome engineering. *Nature Protocols*. 2012;7(1):171–192.

636 27. Foley JE, Yeh J-RJ, Maeder ML, Reyon D, Sander JD, Peterson RT, Joung JK. Rapid Mutation of
637 Endogenous Zebrafish Genes Using Zinc Finger Nucleases Made by Oligomerized Pool ENgineering
638 (OPEN). *PLoS ONE*. 2009;4(2):e4348.

639 28. Wang G, Yang L, Grishin D, Rios X, Ye LY, Hu Y, Li K, Zhang D, Church GM, Pu WT. Efficient,
640 footprint-free human iPSC genome editing by consolidation of Cas9/CRISPR and piggyBac technologies.
641 *Nature Protocols*. 2017;12(1):88–103.

642 29. Guner-Ataman B, Paffett-Lugassy N, Adams MS, Nevis KR, Jahangiri L, Obregon P, Kikuchi K,
643 Poss KD, Burns CE, Burns CG. Zebrafish second heart field development relies on progenitor
644 specification in anterior lateral plate mesoderm and nkx2.5 function. *Development (Cambridge, England)*.
645 2013;140(6):1353–1363.

646 30. Paffett-Lugassy N, Singh R, Nevis KR, Guner-Ataman B, O'Loughlin E, Jahangiri L, Harvey RP,
647 Burns CG, Burns CE. Heart field origin of great vessel precursors relies on nkx2.5-mediated
648 vasculogenesis. *Nature Cell Biology*. 2013;15(11):1362–1369.

649 31. Schoenebeck JJ, Keegan BR, Yelon D. Vessel and blood specification override cardiac potential in
650 anterior mesoderm. *Developmental cell*. 2007;13(2):254–267.

651 32. Serbedzija GN, Chen JN, Fishman MC. Regulation in the heart field of zebrafish. *Development*
652 *(Cambridge, England)*. 1998;125(6):1095–1101.

653 33. Kaufman OH, Lee K, Martin M, Rothhämel S, Marlow FL. rbpms2 functions in Balbiani body
654 architecture and ovary fate. *PLoS genetics*. 2018;14(7):e1007489.

655 34. Gerber WV, Yatskievych TA, Antin PB, Correia KM, Conlon RA, Krieg PA. The RNA-binding
656 protein gene, hermes, is expressed at high levels in the developing heart. *Mechanisms of development*.
657 1999;80(1):77–86.

658 35. Akerberg AA, Burns CE, Burns CG. Exploring the Activities of RBPMS Proteins in Myocardial
659 Biology. *Pediatric cardiology*. 2019;40(7):1410–1418.

660 36. Wilmore HP, McClive PJ, Smith CA, Sinclair AH. Expression profile of the RNA-binding protein
661 gene hermes during chicken embryonic development. *Developmental dynamics : an official publication of*
662 *the American Association of Anatomists*. 2005;233(3):1045–1051.

663 37. Yelon D, Horne SA, Stainier DY. Restricted expression of cardiac myosin genes reveals regulated
664 aspects of heart tube assembly in zebrafish. *Developmental biology*. 1999;214(1):23–37.

665 38. Hörnberg H, Horck FW, Maurus D, Zwart M, Svoboda H, Harris WA, Holt CE. RNA-binding protein
666 Hermes/RBPMS inversely affects synapse density and axon arbor formation in retinal ganglion cells in
667 vivo. *The Journal of neuroscience : the official journal of the Society for Neuroscience*.
668 2013;33(25):10384–10395.

669 39. Pater E de, Clijsters L, Marques SR, Lin Y-F, Garavito-Aguilar ZV, Yelon D, Bakkers J. Distinct
670 phases of cardiomyocyte differentiation regulate growth of the zebrafish heart. *Development (Cambridge,*
671 *England)*. 2009;136(10):1633–1641.

672 40. Lazic S, Scott IC. Mef2cb regulates late myocardial cell addition from a second heart field-like
673 population of progenitors in zebrafish. *Developmental biology*. 2011;354(1):123–133.

674 41. Hami D, Grimes AC, Tsai H-J, Kirby ML. Zebrafish cardiac development requires a conserved
675 secondary heart field. *Development (Cambridge, England)*. 2011;138(11):2389–2398.

676 42. Akerberg AA, Burns CE, Burns CG, Nguyen C. Deep learning enables automated volumetric
677 assessments of cardiac function in zebrafish. *Disease models & mechanisms*. 2019;12(10):dmm040188.

678 43. Cuspidi C, Negri F, Sala C, Valerio C, Mancia G. Association of left atrial enlargement with left
679 ventricular hypertrophy and diastolic dysfunction: A tissue Doppler study in echocardiographic practice.
680 *Blood Pressure*. 2011;21(1):24–30.

681 44. Cuspidi C, Rescaldani M, Sala C. Prevalence of Echocardiographic Left-Atrial Enlargement in
682 Hypertension: A Systematic Review of Recent Clinical Studies. *American Journal of Hypertension*.
683 2013;26(4):456–464.

684 45. Huttner IG, Wang LW, Santiago CF, Horvat C, Johnson R, Cheng D, Frieling-Salewsky M von,
685 Hillcoat K, Bemand TJ, Trivedi G, Braet F, Hesselson D, Alford K, Hayward CS, Seidman JG, et al. A-
686 Band Titin Truncation in Zebrafish Causes Dilated Cardiomyopathy and Hemodynamic Stress
687 Intolerance. *Circulation: Genomic and Precision Medicine*. 2018;11(8):e002135.

688 46. Horsthuis T, Houweling AC, Habets PEMH, Lange FJ de, Azzouzi H el, Clout DEW, Moorman
689 AFM, Christoffels VM. Distinct regulation of developmental and heart disease-induced atrial natriuretic
690 factor expression by two separate distal sequences. *Circulation research*. 2008;102(7):849–859.

691 47. Grassini DR, Lagendijk AK, Angelis JED, Silva JD, Jeanes A, Zettler N, Bower NI, Hogan BM,
692 Smith KA. Nppa and Nppb act redundantly during zebrafish cardiac development to confine AVC marker
693 expression and reduce cardiac jelly volume. *Development (Cambridge, England)*.
694 2018;145(12):dev160739.

695 48. Berdougo E, Coleman H, Lee DH, Stainier DYR, Yelon D. Mutation of weak atrium/atrial myosin
696 heavy chain disrupts atrial function and influences ventricular morphogenesis in zebrafish. *Development*
697 *(Cambridge, England)*. 2003;130(24):6121–6129.

698 49. Nakagaki-Silva EE, Gooding C, Llorian M, Jacob AG, Richards F, Buckroyd A, Sinha S, Smith CW.
699 Identification of RBPMS as a mammalian smooth muscle master splicing regulator via proximity of its
700 gene with super-enhancers. *eLife*. 2019;8.

701 50. Shen S, Park JW, Lu Z, Lin L, Henry MD, Wu YN, Zhou Q, Xing Y. rMATS: robust and flexible
702 detection of differential alternative splicing from replicate RNA-Seq data. *Proceedings of the National*
703 *Academy of Sciences of the United States of America*. 2014;111(51):E5593-601.

704 51. Agarkova I, Perriard J-C. The M-band: an elastic web that crosslinks thick filaments in the center of
705 the sarcomere. *Trends in Cell Biology*. 2005;15(9):477–485.

706 52. Gautel M, Djinović-Carugo K. The sarcomeric cytoskeleton: from molecules to motion. *Journal of*
707 *Experimental Biology*. 2016;219(2):135–145.

708 53. Previs MJ, Previs SB, Gulick J, Robbins J, Warshaw DM. Molecular Mechanics of Cardiac Myosin-
709 Binding Protein C in Native Thick Filaments. *Science*. 2012;337(6099):1215–1218.

710 54. Previs MJ, Prosser BL, Mun JY, Previs SB, Gulick J, Lee K, Robbins J, Craig R, Lederer WJ,
711 Warshaw DM. Myosin-binding protein C corrects an intrinsic inhomogeneity in cardiac excitation-
712 contraction coupling. *Science Advances*. 2015;1(1):e1400205.

713 55. Ebert AM, Hume GL, Warren KS, Cook NP, Burns CG, Mohideen MA, Siegal G, Yelon D, Fishman
714 MC, Garrity DM. Calcium extrusion is critical for cardiac morphogenesis and rhythm in embryonic

715 zebrafish hearts. *Proceedings of the National Academy of Sciences of the United States of America*.
716 2005;102(49):17705–17710.

717 56. Langenbacher AD, Dong Y, Shu X, Choi J, Nicoll DA, Goldhaber JI, Philipson KD, Chen J-N.
718 Mutation in sodium–calcium exchanger 1 (NCX1) causes cardiac fibrillation in zebrafish. *Proceedings of*
719 *the National Academy of Sciences of the United States of America*. 2005;102(49):17699–17704.

720 57. Katz Y, Wang ET, Airoldi EM, Burge CB. Analysis and design of RNA sequencing experiments for
721 identifying isoform regulation. *Nature Methods*. 2010;7(12):1009–1015.

722 58. McNamara JW, Sadayappan S. Skeletal myosin binding protein-C: An increasingly important
723 regulator of striated muscle physiology. *Archives of Biochemistry and Biophysics*. 2018;660:121–128.

724 59. Gautel M, Zuffardi O, Freiburg A, Labeit S. Phosphorylation switches specific for the cardiac isoform
725 of myosin binding protein-C: a modulator of cardiac contraction? *The EMBO Journal*. 1995;14(9):1952–
726 1960.

727 60. Mohamed AS, Dignam JD, Schlender KK. Cardiac Myosin-Binding Protein C (MyBP-C):
728 Identification of Protein Kinase A and Protein Kinase C Phosphorylation Sites. *Archives of Biochemistry*
729 *and Biophysics*. 1998;358(2):313–319.

730 61. Kofuji P, Lederer WJ, Schulze DH. Mutually exclusive and cassette exons underlie alternatively
731 spliced isoforms of the Na/Ca exchanger. *Journal of Biological Chemistry*. 1994;269(7):5145–5149.

732 62. Quednau BD, Nicoll DA, Philipson KD. Tissue specificity and alternative splicing of the Na+/Ca2+
733 exchanger isoforms NCX1, NCX2, and NCX3 in rat. *American Journal of Physiology-Cell Physiology*.
734 1997;272(4):C1250–C1261.

735 63. Simmerman HKB, Jones LR. Phospholamban: Protein Structure, Mechanism of Action, and Role in
736 Cardiac Function. *Physiological Reviews*. 1998;78(4):921–947.

737 64. Toyoshima C, Asahi M, Sugita Y, Khanna R, Tsuda T, MacLennan DH. Modeling of the inhibitory
738 interaction of phospholamban with the Ca2+ ATPase. *Proceedings of the National Academy of Sciences*.
739 2003;100(2):467–472.

740 65. Koushik SV, Wang J, Rogers R, Moskophidis D, Lambert NA, Creazzo TL, Conway SJ. Targeted
741 inactivation of the sodium-calcium exchanger (Ncx1) results in the lack of a heartbeat and abnormal
742 myofibrillar organization. *The FASEB Journal*. 2001;15(7):1209–1211.

743 66. Russell JT. Imaging calcium signals in vivo: a powerful tool in physiology and pharmacology. *British*
744 *Journal of Pharmacology*. 2011;163(8):1605–1625.

745 67. Kosaka K, Kawakami K, Sakamoto H, Inoue K. Spatiotemporal localization of germ plasm RNAs
746 during zebrafish oogenesis. *Mechanisms of Development*. 2007;124(4):279–289.

747 68. Heim AE, Hartung O, Rothhämel S, Ferreira E, Jenny A, Marlow FL. Oocyte polarity requires a
748 Bucky ball-dependent feedback amplification loop. *Development*. 2014;141(4):842–854.

749 69. Farazi TA, Leonhardt CS, Mukherjee N, Mihailovic A, Li S, Max KEA, Meyer C, Yamaji M, Cekan
750 P, Jacobs NC, Gerstberger S, Bognanni C, Larsson E, Ohler U, Tuschl T. Identification of the RNA
751 recognition element of the RBPMS family of RNA-binding proteins and their transcriptome-wide mRNA
752 targets. *RNA (New York, N.Y.)*. 2014;20(7):1090–1102.

753 70. Notarnicola C, Rouleau C, Guen LL, Virsolvy A, Richard S, Faure S, Barbara PDS. The RNA-
754 Binding Protein RBPMS2 Regulates Development of Gastrointestinal Smooth Muscle. *Gastroenterology*.
755 2012;143(3):687-697.e9.

756 71. Furukawa MT, Sakamoto H, Inoue K. Interaction and colocalization of HERMES/RBPMS with
757 NonO, PSF, and G3BP1 in neuronal cytoplasmic RNP granules in mouse retinal line cells. *Genes to*
758 *Cells*. 2015;20(4):257–266.

759 72. Quinlan AR, Hall IM. BEDTools: a flexible suite of utilities for comparing genomic features.
760 *Bioinformatics*. 2010;26(6):841–842.

761 73. Patro R, Duggal G, Love MI, Irizarry RA, Kingsford C. Salmon provides fast and bias-aware
762 quantification of transcript expression. *Nature Methods*. 2017;14(4):417–419.

763 74. Soneson C, Love MI, Robinson MD. Differential analyses for RNA-seq: transcript-level estimates
764 improve gene-level inferences. *F1000Research*. 2016;4:1521.

765 75. Dobin A, Davis CA, Schlesinger F, Drenkow J, Zaleski C, Jha S, Batut P, Chaisson M, Gingeras TR.
766 STAR: ultrafast universal RNA-seq aligner. *Bioinformatics*. 2013;29(1):15–21.

767 76. Li B, Dewey CN. RSEM: accurate transcript quantification from RNA-Seq data with or without a
768 reference genome. *BMC Bioinformatics*. 2011;12(1):323.

769 77. Love MI, Huber W, Anders S. Moderated estimation of fold change and dispersion for RNA-seq data
770 with DESeq2. *Genome Biology*. 2014;15(12):550.

771 78. Katz Y, Wang ET, Silterra J, Schwartz S, Wong B, Thorvaldsdóttir H, Robinson JT, Mesirov JP,
772 Airoldi EM, Burge CB. Quantitative visualization of alternative exon expression from RNA-seq data.
773 *Bioinformatics*. 2015;31(14):2400–2402.

774 79. Thisse C, Thisse B. High-resolution in situ hybridization to whole-mount zebrafish embryos. *Nature*
775 *protocols*. 2008;3(1):59–69.

776 80. Schneider CA, Rasband WS, Eliceiri KW. NIH Image to ImageJ: 25 years of image analysis. *Nature*
777 *methods*. 2012;9(7):671–675.

778 81. Jahangiri L, Sharpe M, Novikov N, González-Rosa JM, Borikova A, Nevis K, Paffett-Lugassy N,
779 Zhao L, Adams M, Guner-Ataman B, Burns CE, Burns CG. The AP-1 transcription factor component
780 Fosl2 potentiates the rate of myocardial differentiation from the zebrafish second heart field.
781 *Development*. 2016;143(1):113–122.

782 82. Poss KD, Wilson LG, Keating MT. Heart Regeneration in Zebrafish. *Science*. 2002;298(5601):2188–
783 2190.

784 83. Akerberg AA, Henner A, Stewart S, Stankunas K. Histone demethylases Kdm6ba and Kdm6bb
785 redundantly promote cardiomyocyte proliferation during zebrafish heart ventricle maturation.
786 *Developmental Biology*. 2017;426(1):84–96.

787 84. Power RM, Huisken J. A guide to light-sheet fluorescence microscopy for multiscale imaging. *Nature*
788 *Methods*. 2017;14(4):360–373.

789 85. Huisken J, Stainier DYR. Even fluorescence excitation by multidirectional selective plane
790 illumination microscopy (mSPIM). *Optics Letters*. 2007;32(17):2608.

791 86. Livak KJ, Schmittgen TD. Analysis of relative gene expression data using real-time quantitative PCR
792 and the 2(-Delta Delta C(T)) Method. *Methods (San Diego, Calif.)*. 2001;25(4):402–408.

793 87. Panáková D, Werdich AA, MacRae CA. Wnt11 patterns a myocardial electrical gradient through
794 regulation of the L-type Ca(2+) channel. *Nature*. 2010;466(7308):874–878.

795

796

797 **FIGURES AND LEGENDS**

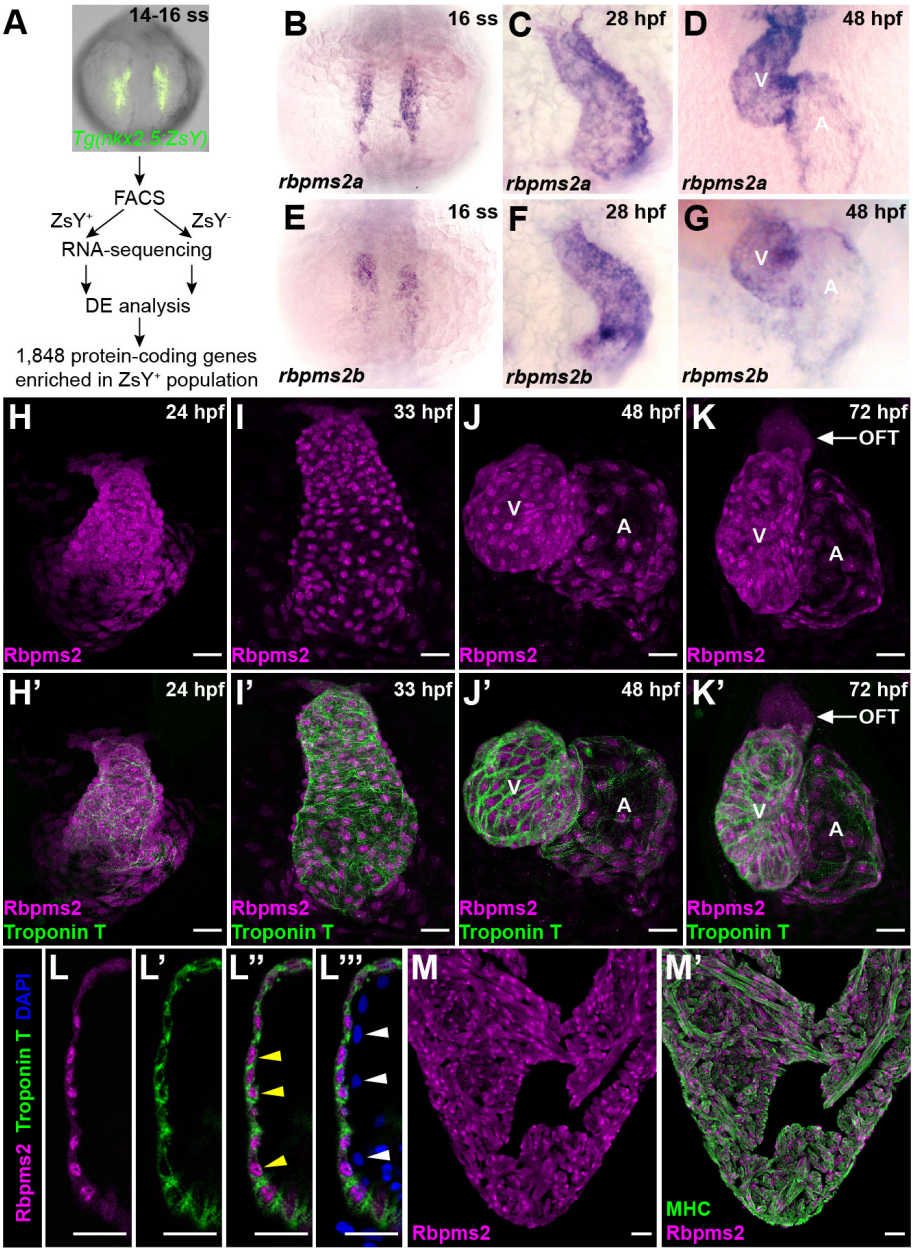

798

799 **Figure 1 – Restricted expression of RNA-binding proteins Rbpms2a and Rbpms2b to the**
800 **zebrafish myocardium.** (A) Workflow used to identify 1848 protein-coding RNAs enriched in
801 ZsYellow-positive (ZsY+) cardiopharyngeal progenitors or cardiomyocytes in the anterior lateral
802 plate mesoderm of 14-16 somite stage (ss) *Tg(nkx2.5:ZsYellow)* embryos. (B-G) Brightfield
803 images of 16 ss (B,E), 28 hours post fertilization (hpf; C,F), and 48 hpf (D,G) embryos
804 processed for in situ hybridization with riboprobes that detect *rbpms2a* (B-D) or *rbpms2b* (E-G).
805 Little to no variation in expression pattern was observed between animals in each group
806 (n>10/group). (H-K') Confocal projections of hearts in 24 hpf (H,H'), 33 hpf (I,I'), 48 hpf (J,J'),

807 and 72 hpf (K,K') zebrafish embryos co-immunostained with antibodies that detect Rbpms2
808 (magenta) or cardiac Troponin T (CT3 antibody; green). Single (H,I,J,K) and merged double
809 channel (H',I',J',K') images are shown. Little to no variation in expression pattern was observed
810 between animals in each group (n>10/group). (L-L''') Single optical section through the
811 ventricular wall of a 48 hpf embryo co-immunostained with antibodies that detect Rbpms2
812 (magenta) or cardiac Troponin T (CT3 antibody; green) and counterstained with DAPI (blue).
813 Single (L, L'), merged double (L''), and merged triple (L''') channel images are shown. Yellow
814 arrowheads highlight Rbpms2-positive cardiomyocyte nuclei surrounded by Troponin T-positive
815 cytoplasm. White arrowheads highlight Rbpms2-negative nuclei in adjacent endocardial cells
816 lining the ventricular chamber. 4/4 ventricles exhibited this Rbpms2 expression pattern. (M,M')
817 Confocal projections of a histological section through the ventricle of an adult zebrafish heart co-
818 immunostained with antibodies that detect Rbpms2 (magenta) or Myosin Heavy Chain (MHC;
819 MF20 antibody; green). Single channel (M) and merged double channel (M') images are shown.
820 18/18 sections, 6 from each of three hearts, exhibited this Rbpms2 expression pattern.
821 Abbreviations: FACS, fluorescence activated cell sorting, DE, differential expression; V,
822 ventricle; A, atrium; OFT, outflow tract. Scale bars=25μm.

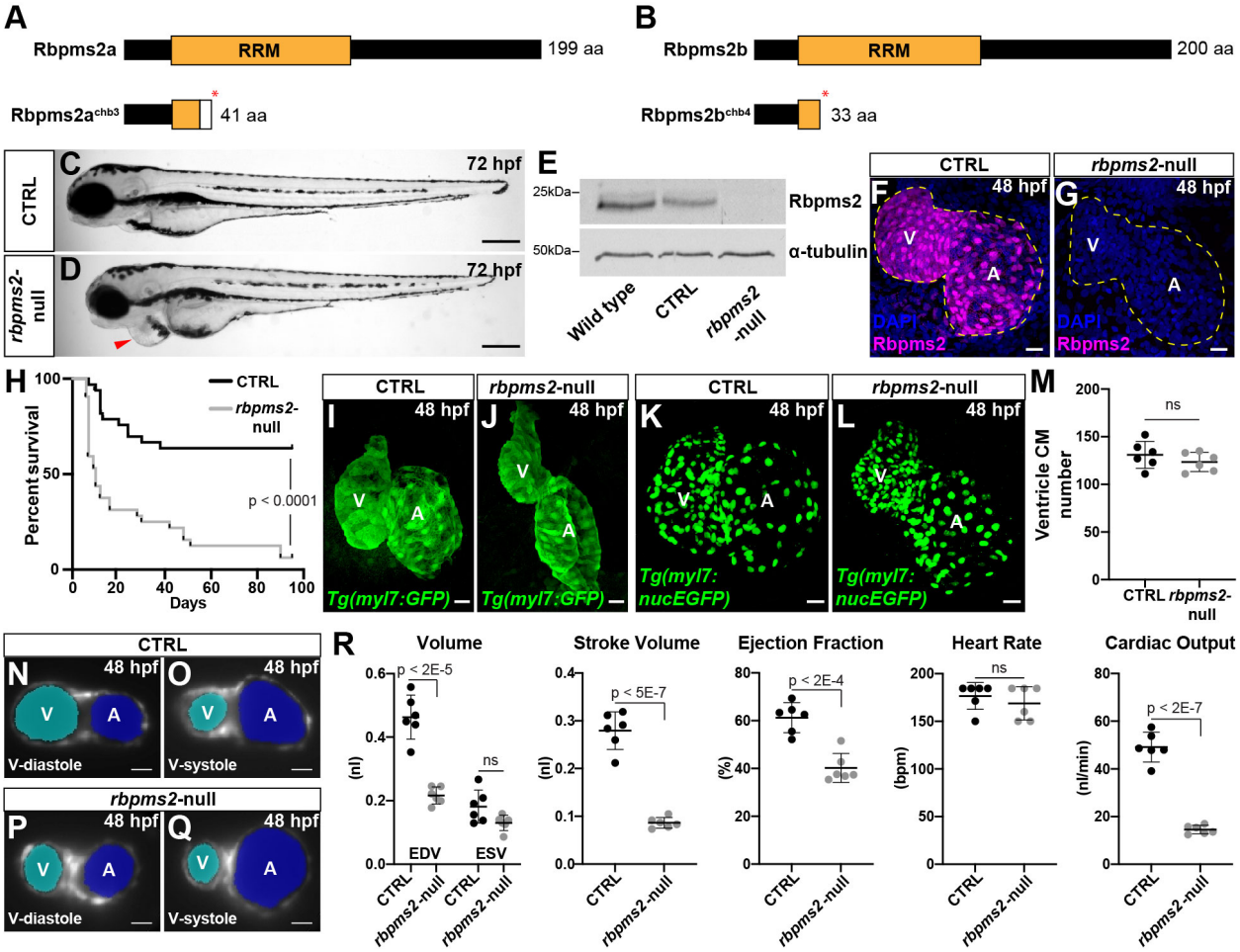

Figure 2 – *rbpms2a* and *rbpms2b* are required for ventricular function. (A,B) Schematic diagrams of Rbpms2a and Rbpms2b (top) and the predicted protein products of the *rbpms2a*^{chb3} and *rbpms2b*^{chb4} alleles (bottom). The asterisks mark the locations of premature stop codons (*) within the RNA-recognition motifs (RRMs) caused by frame-shifting deletions. The white box in (A) shows the location of divergent amino acids prior to the stop codon. (C-D) Brightfield images of control-sibling (C; CTRL) and *rbpms2*-null (*rbpms2a*$^{chb3/chb3}$; *rbpms2b*$^{chb4/chb4}$; D) embryos at 72 hours post fertilization (hpf). Arrowhead highlights pericardial edema in the mutant. Little to no variation in phenotype was observed between animals in each group (n>10/group). Scale bars=250μm. (E) Western blot showing Rbpms2 levels in 48 hpf wild-type (WT), CTRL, and *rbpms2*-null embryos (top) relative to the loading control alpha-tubulin (bottom). (F-G) Confocal projections of hearts in 48 hpf CTRL (F) and *rbpms2*-null (G) embryos immunostained with an antibody that detects Rbpms2 (magenta) and counterstained with DAPI (blue). The dotted lines delineate the myocardium as ascertained from the Rbpms2 signal (F) or *Tg(myl7:eGFP)* reporter signal present in these animals (F,G; not shown). Little to no variation in expression pattern was observed between animals in each group (n>10/group). (H) Kaplan Meier plot

839 showing the survival curves of CTRL (n=33) and *rbpms2*-null (n=33) animals. Statistical
840 significance was determined using a log-rank test. (I-L) Confocal projections of hearts in 48 hpf
841 CTRL (I,K) or *rbpms2*-null (J,L) embryos carrying the *myl7:GFP* (I,J) or *myl7:nucGFP* (K,L)
842 transgenes immunostained with an anti-GFP antibody. For (I,J), little to no variation in
843 phenotype was observed between animals in each group (n>10/group). (M) Dot plot showing
844 ventricular cardiomyocyte (CM) number in CTRL (n=6) and *rbpms2*-null (n=6) hearts at 48 hpf.
845 Error bars show one standard deviation. Statistical significance was determined by an unpaired,
846 two-tailed Student's t-test assuming equal variances. ns, not significant. (N-Q) Representative
847 single-plane light sheet fluorescence microscopy images of hearts in 48 hpf CTRL (N,O) and
848 *rbpms2*-null (P,Q) embryos carrying the *myl7:GFP* transgene. Images of hearts during
849 ventricular diastole (N,P) or systole (O,Q) are shown with Cardiac Functional Imaging Network
850 (CFIN) overlays of the atrial (blue) and ventricular (cyan) lumens. (R) Dot plots showing end-
851 diastolic volume (EDVs) and end-systolic volume (ESVs), stroke volume, ejection fraction, heart
852 rate, and cardiac output of ventricles in 48 hpf CTRL (n=6) and *rbpms2*-null (n=6) animals
853 measured with CFIN. Error bars show one standard deviation. Statistical significance was
854 determined by an unpaired, two-tailed Student's t-test assuming equal variances. ns, not
855 significant. Abbreviations: aa, amino acid; V, ventricle; A, atrium. Scale bars=25μm.
856

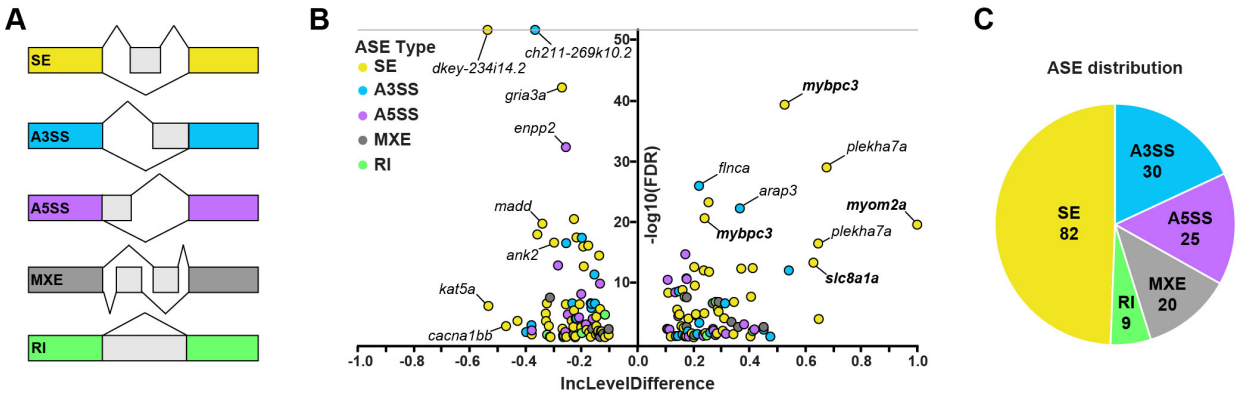

Figure 3 – Identification of differential alternative splicing events in *rbpms2*-null embryos. (A) Schematic diagrams of the categories of alternative splicing events (ASEs) investigated by the RNA-seq Multivariate Analysis of Transcript Splicing (rMATS) algorithm including skipped exon (SE), alternative 3' splice site (A3SS), alternative 5' splice site (A5SS), mutually exclusive exon (MXE), and retained intron (RI). (B) Volcano plot showing the inclusion (Inc) level differences (control-sibling Inclevel - *rbpms2*-null Inclevel) and False Discovery Rates (FDR) for differential ASEs between 33 hours post fertilization (hpf) control-sibling and *rbpms2*-null animals (0 uncalled replicates; FDR<0.01; |Incleveldifference|>0.1;). The ASEs shown in bold were validated with splicing-sensitive qPCR and in situ hybridization. (C) Pie chart showing the proportions of differential ASEs in each category in *rbpms2*-null animals.

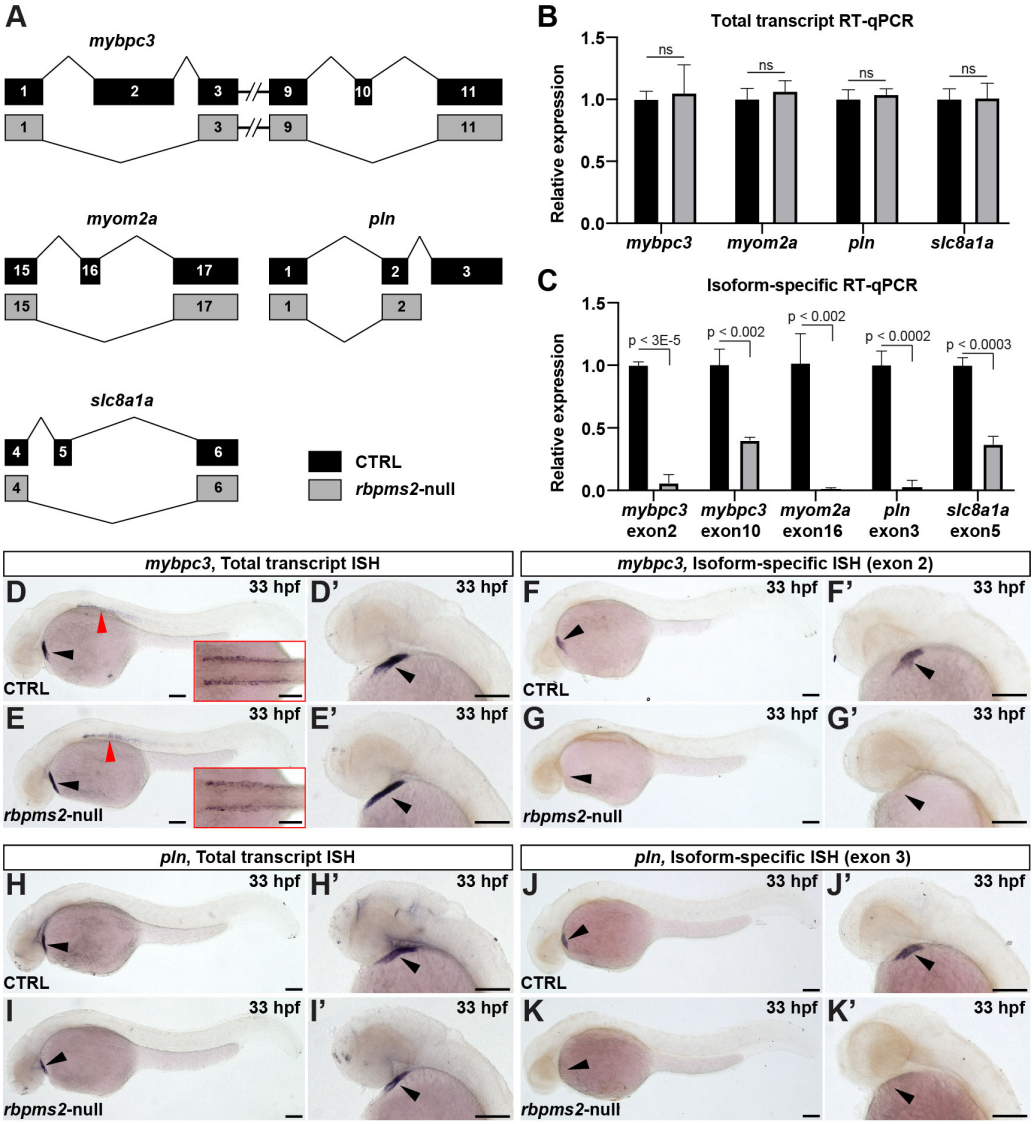

Figure 4 – Validation of differential alternative splicing events in *rbpms2*-null animals. (A) Schematic diagrams of alternative splicing events (ASEs) identified in control-sibling (CTRL) or *rbpms2*-null animals at 33 hours post fertilization (hpf) by the RNA-seq Multivariate Analysis of Transcript Splicing (rMATS) or mixture of isoforms (MISO) algorithms. The legend indicates that the isoforms shown on top (black) are significantly reduced or absent in *rbpms2*-null animals and replaced by the isoforms shown on the bottom (gray). (B) Bar graph showing the relative expression levels of the four genes shown in (A), independent of the alternatively spliced exons, between 48 hours post fertilization control-sibling and DKO animals. (C) Bar graph showing the relative expression levels of the indicated, exon-containing isoforms [(shown in black in (A)] of the same four genes between control-sibling and *rbpms2*-null animals at 48 hpf. For (B,C), error bars show one standard deviation. Statistical significance was determined by an unpaired, two-

881 tailed Student's t-test assuming equal variances. ns, not significant. (D-K') Brightfield images of
882 33 hpf CTRL (D,D',F,F',H,H'J,J') and *rbpms2*-null (E,E',G,G',I,I',K,K') embryos processed for in
883 situ hybridization with riboprobes that detect total pools (D-E'; H-I') or specific exon-containing
884 mRNA isoforms (F-G'; J-K') of *mybpc3* (D-G') or *pln* (H-K'). The cardiac regions in
885 (D,E,F,G,H,I,J,K) are shown at higher zoom in (D',E',F',G',H',I',J',K'). Red arrowheads in (D,E)
886 highlight expression of *mybpc3* in skeletal muscle, which is shown from a dorsal view in the
887 insets. Black arrowheads in (D-K) indicate the linear heart tube. Little to no variation in
888 expression pattern was observed between animals in each group (n>10/group). Scale
889 bars=100μm.
890

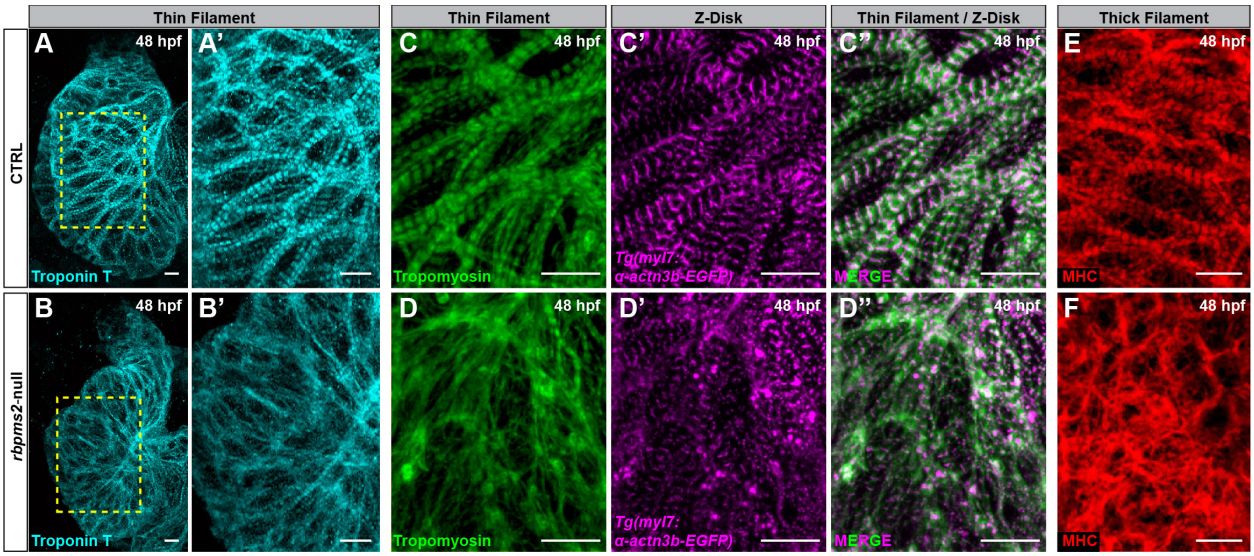

Figure 5 – Myofibrillar disarray in *rbpms2*-null ventricular cardiomyocytes. (A-B') Confocal projections of ventricles in 48 hours post fertilization (hpf) control-sibling (CTRL) or *rbpms2*-null embryos immunostained with an anti-TroponinT antibody (CT3) to visualize thin filaments. Regions demarcated in (A) and (B) are enlarged in (A') and (B'). (C-D'') Confocal projections of ventricles in 48 hpf CTRL and *rbpms2*-null *Tg(α-actn3b-EGFP)* animals co-immunostained with antibodies that detect Tropomyosin (CH1; green) to visualize thin filaments or GFP (magenta) to visualize Z-disks. (E-F) Confocal projections of ventricles in 48 hpf CTRL and *rbpms2*-null embryos immunostained with an antibody that detects myosin heavy chain (MF20) to visualize thick filaments. Little to no variation in protein distributions were observed between animals in each group (n>10 animals/group). Scale bars=10μm.

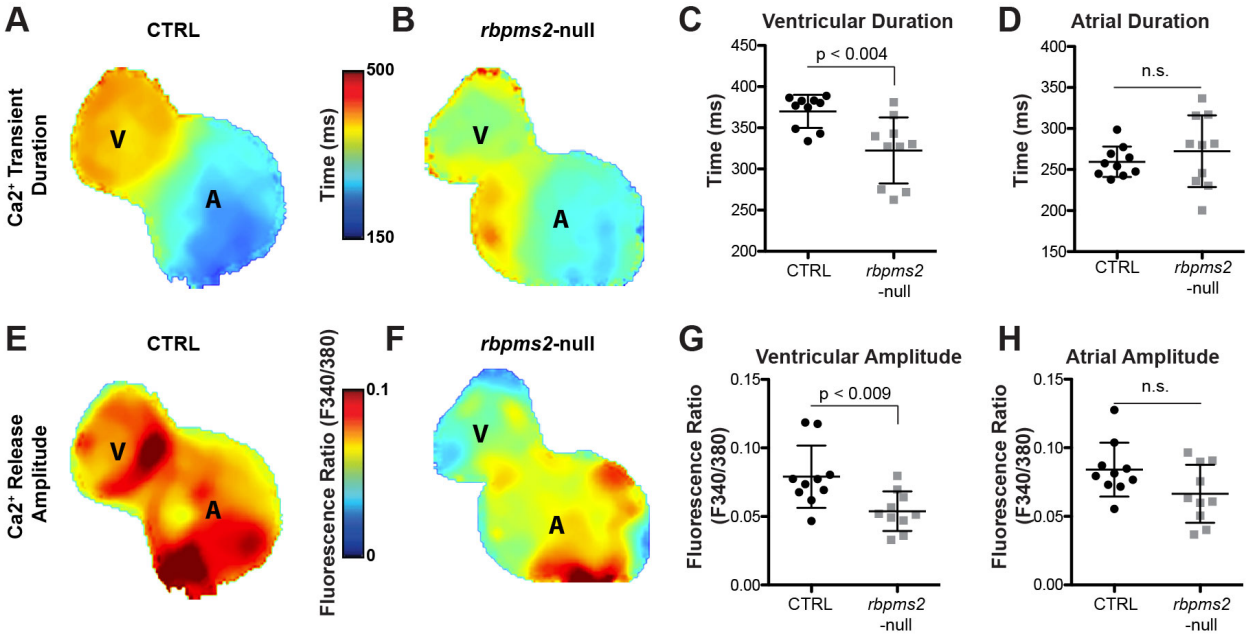

Figure 6 – *rbpms2*-null ventricular cardiomyocytes exhibit reductions in Ca2+-transient duration and amplitude. Color maps (A,B,E,F) and dot plots (C,D,G,H; n=10/group) of Ca2+-transient duration (A-D) and Ca2+ release amplitude (E-F) in the ventricle (A-C; E-G) and atrium (A,B,D,E,F,H) of 48 hours post fertilization control-sibling (CTRL; A,C,D,E,G,H) and *rbpms2*-null (B-D; F-H) hearts. Color code depicts localized Ca2+-transient duration in milliseconds (ms; A,B) or the ratiometric fluorescence indicator of Ca2+-release amplitude. Each dot represents center-chamber measurements from one heart. Error bars show one standard deviation. Statistical significance was determined by an unpaired, two-tailed Student's t-test assuming equal variances. ns, not significant.

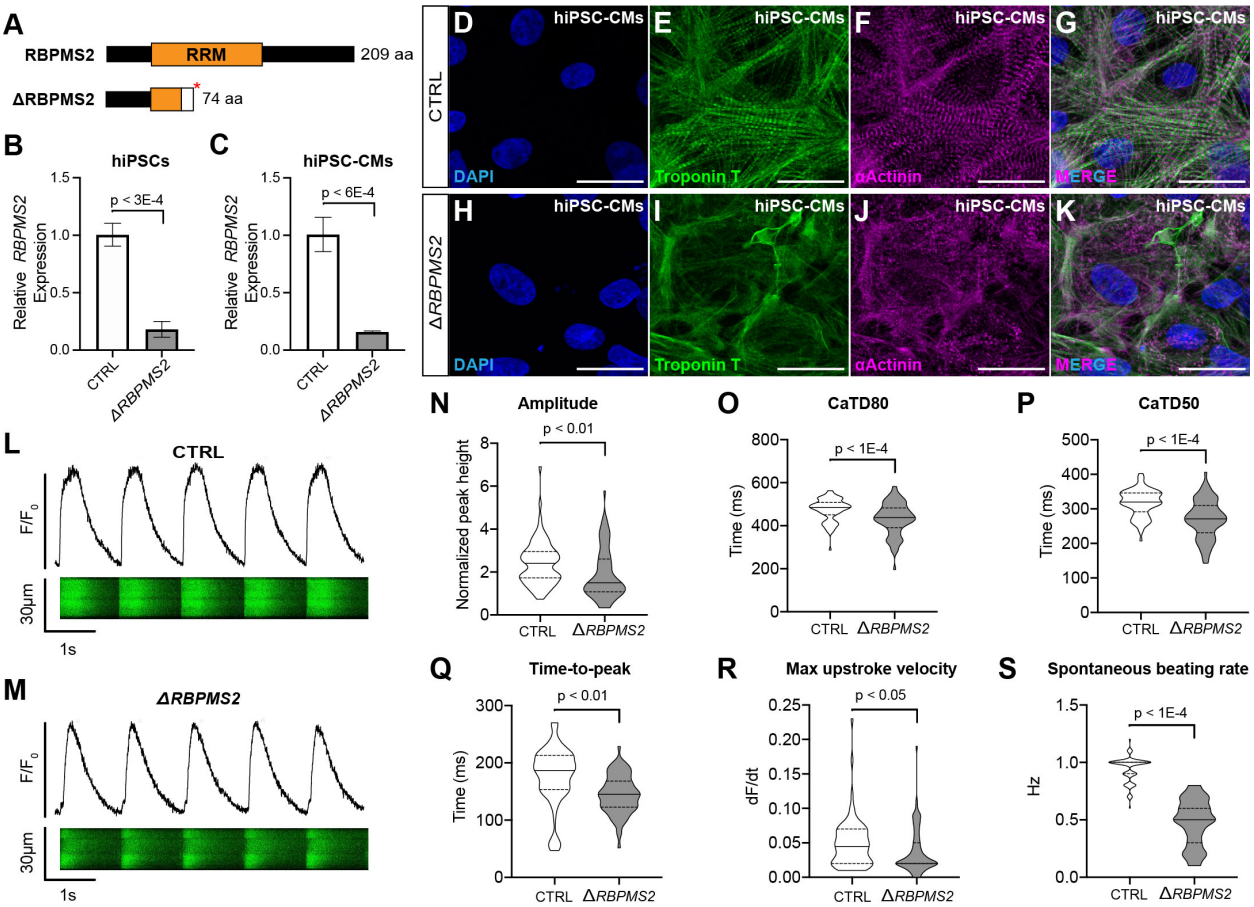

Figure 7 – Human *RBPMS2*-null cardiomyocytes exhibit myofibrillar disarray and Ca2+ handling defects similar to those in zebrafish *rbpms2*-null cardiomyocytes. (A,B) Schematic diagrams of human RBPMS2 (top) and the predicted protein product of the *ΔRBPMS2* null allele created with CRISPR/Cas9-mediated genome editing (bottom). The asterisk shows the location of a premature stop codon within the RNA-recognition motif (RRM) caused by a frame-shifting 2 base pair deletion. The white box shows the location of divergent amino acids prior to the stop codon. (B,C) Bar graphs showing the relative expression levels of *RBPMS2* in parental control (CTRL) and *ΔRBPMS2* human induced pluripotent stem cells (hiPSCs; B) and cardiomyocytes (hiPSC-CMs; C) after 15 days of directed differentiation. Error bars show one standard deviation. Statistical significance was determined by an unpaired, two-tailed Student's t-test assuming equal variances. (D-K) Representative confocal projections of CTRL (D-G) and *ΔRBPMS2* (H-K) hiPSC-CMs immunostained with antibodies that detect TroponinT (CT3; green) or Alpha Actinin (anti-Sarcomeric Alpha Actinin; magenta) to visualize thin filaments or Z-disks, respectively, and counterstained with DAPI (blue). Single (D-F; H-J) and merged triple (G,K) channel images are shown. Little to no variation in staining pattern was observed between cells in each experimental group (n>50 cells/group from at least three wells

931 from two separate differentiations were examined). (L,M) Representative traces of fluorescence
932 intensity over baseline (F/F_o; top) derived from line scans (bottom) of CTRL (L) and *ΔRBPMS2*
933 (M) hiPSC-CMs loaded with fluo-4 and paced at 1Hz. (N-S) Violin plots showing Ca2+-transient
934 amplitude (N), duration at 80% (O) and 50% (P) repolarization, time to peak amplitude (Q),
935 upstroke velocity (R), and un-paced spontaneous beating rate (S). Statistical significance was
936 determined by an unpaired, two-tailed Student's t-test assuming equal variances. n=80
937 cells/group, 40 each from two separate differentiations. Scale bars=25μm.